NASA/TP-1999-209694

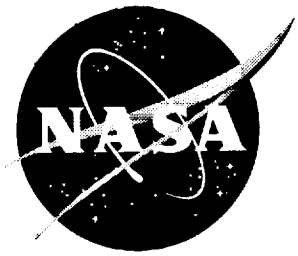

Concept Development of a Mach 2.4 High-Speed Civil Transport

James W. Fenbert
Langley Research Center, Hampton, Virginia

Lori P. Ozoroski, Karl A. Geiselhart, and Elwood W. Shields
Lockheed Engineering & Sciences Company, Hampton, Virginia

Marcus O. McElroy
Langley Research Center, Hampton, Virginia

December 1999

The NASA STI Program Office . . . in Profile

Since its founding, NASA has been dedicated to the advancement of aeronautics and space science. The NASA Scientific and Technical Information (STI) Program Office plays a key part in helping NASA maintain this important role.

The NASA STI Program Office is operated by Langley Research Center, the lead center for NASA's scientific and technical information. The NASA STI Program Office provides access to the NASA STI Database, the largest collection of aeronautical and space science STI in the world. The Program Office is also NASA's institutional mechanism for disseminating the results of its research and development activities. These results are published by NASA in the NASA STI Report Series, which includes the following report types:

- TECHNICAL PUBLICATION. Reports of completed research or a major significant phase of research that present the results of NASA programs and include extensive data or theoretical analysis. Includes compilations of significant scientific and technical data and information deemed to be of continuing reference value. NASA counterpart of peer-reviewed formal professional papers, but having less stringent limitations on manuscript length and extent of graphic presentations.

- TECHNICAL MEMORANDUM. Scientific and technical findings that are preliminary or of specialized interest, e.g., quick release reports, working papers, and bibliographies that contain minimal annotation. Does not contain extensive analysis.

- CONTRACTOR REPORT. Scientific and technical findings by NASA-sponsored contractors and grantees.

- CONFERENCE PUBLICATION. Collected papers from scientific and technical conferences, symposia, seminars, or other meetings sponsored or co-sponsored by NASA.

- SPECIAL PUBLICATION. Scientific, technical, or historical information from NASA programs, projects, and missions, often concerned with subjects having substantial public interest.

- TECHNICAL TRANSLATION. English-language translations of foreign scientific and technical material pertinent to NASA's mission.

Specialized services that complement the STI Program Office's diverse offerings include creating custom thesauri, building customized databases, organizing and publishing research results . . . even providing videos.

For more information about the NASA STI Program Office, see the following:

- Access the NASA STI Program Home Page at ***http://www.sti.nasa.gov***

- Email your question via the Internet to help@sti.nasa.gov

- Fax your question to the NASA STI Help Desk at (301) 621-0134

- Telephone the NASA STI Help Desk at (301) 621-0390

- Write to:
  NASA STI Help Desk
  NASA Center for AeroSpace Information
  7121 Standard Drive
  Hanover, MD 21076-1320

NASA/TP-1999-209694

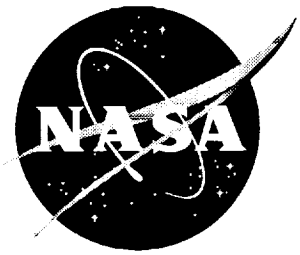

Concept Development of a Mach 2.4 High-Speed Civil Transport

James W. Fenbert
Langley Research Center, Hampton, Virginia

Lori P. Ozoroski, Karl A. Geiselhart, and Elwood W. Shields
Lockheed Engineering & Sciences Company, Hampton, Virginia

Marcus O. McElroy
Langley Research Center, Hampton, Virginia

National Aeronautics and
Space Administration

Langley Research Center
Hampton, Virginia 23681-2199

December 1999

Available from:

NASA Center for AeroSpace Information (CASI)
7121 Standard Drive
Hanover, MD 21076-1320
(301) 621-0390

National Technical Information Service (NTIS)
5285 Port Royal Road
Springfield, VA 22161-2171
(703) 605-6000

Summary

In support of the NASA High-Speed Research Program, a Mach 2.4 high-speed civil transport concept was developed to serve as a baseline for studies to assess advanced technologies required for a feasible year 2005 entry-into-service vehicle. The configuration was designed to carry 251 passengers at Mach 2.4 cruise with a 6500-n.mi. range and operate in the existing world airport structure. The details of the configuration development, aerodynamic design, propulsion system and integration, mass properties, sizing, and mission performance are presented. The baseline configuration has a wing area of 9100 ft^2 and a takeoff gross weight of 614 300 lb. The four NASA-defined advanced turbine bypass engines have 39 000 lb thrust with a weight of 9950 lb each. These engines have axisymmetric mixer-ejector nozzles that are assumed to yield 20 dB of noise suppression during takeoff. This level of suppression is assumed adequate to satisfy FAR Stage III noise requirements. The vehicle takeoff thrust-to-weight ratio is 0.254, and the takeoff wing loading is 67.5 lb/ft^2. The configuration was sized by the 11 000-ft takeoff field length requirement and the usable fuel volume limit, which results in a rotation speed of 179 knots and an end-of-mission landing approach velocity of 134 knots. A resizing of the baseline configuration using an engine with a projected life of 9000 hr for hot rotating parts and 18 000 hr for the rest of the engine as required for commercial use on a year 2005 entry-into-service vehicle was also performed. Results show an increase in vehicle takeoff gross weight of approximately 138 000 lb due to these heavier and less efficient engines.

Introduction

In support of the NASA High-Speed Research (HSR) Program, a series of baseline configurations is being developed covering a cruise Mach number range of 1.6 to 2.4, with Mach 2.4 being the focus of the present paper. Economic studies and technology availability estimates of reference 1 indicate Mach 2.4 to be the most promising cruise Mach number for a feasible year 2005 entry-into-service (EIS) vehicle. The details of the design of a NASA-developed Mach 2.4 cruise configuration are presented herein.

Because the configuration being developed was to be used as a baseline, it was necessary to keep the design generically representative to facilitate quick assessments of technologies. The design was developed with a double trapezoidal panel wing planform and without extensive wing/body blending. For this initial baseline development, the configuration was optimized for minimum weight with an all-supersonic design mission without regard for sonic boom levels. Low sonic boom designs can be compared with this configuration to assess the performance penalties for low sonic boom. The increased importance of community takeoff and landing noise constraints on future vehicles influenced the planform design, placing an increased emphasis on low-speed performance over earlier NASA configurations (ref. 2 gives a typical example). The approach was to design a tailless configuration for low weight and high aerodynamic efficiency at cruise, to which a horizontal tail or canard could be added if necessary for control or increased takeoff efficiency. Engine nacelles were axisymmetric, single engine, underwing pods. The baseline technology level selected was intended to reflect that available for service entry in the year 2005. This level of technology was represented in the assumptions of advanced flight control and engine performance characteristics and reduced aircraft structural and systems weights.

The design mission for the Mach 2.4 concept was set at 6500 n.mi. with an all-supersonic cruise. The design passenger load was approximately 250, which could be increased as warranted by the introduction of advanced technologies while maintaining the vehicle size and takeoff gross weight (TOGW). The vehicle was required to be able to operate out of today's major airports, which resulted in a takeoff field length (TOFL) limit of 11 000 ft, and the maximum final approach speed was limited to 160 knots or less while maintaining standard reserve requirements. Current Federal Aviation Regulations require flaps to be fixed during takeoff and landing. For a year 2005 EIS vehicle, automated computer control of the flap system is being introduced to optimize aerodynamic performance and reduce community noise. Center-of-gravity control by pumping fuel would be used during the mission. Landing requirements would be met for a vehicle end-of-mission weight equal to the zero-fuel weight plus reserve fuel.

The development of a Mach 2.4 high-speed civil transport concept is presented in this paper. Advanced propulsion, structures, controls, and aerodynamics are employed in the concept, several of which would require challenging technology development programs to meet the technology availability date for a 2005 EIS vehicle. Details of the design development, aerodynamic design, propulsion system and integration, mass properties, sizing, and mission performance are presented.

Symbols

b	wingspan
C_D	drag coefficient, D/qS

C_L	lift coefficient, L/qS
c	chord
D	drag, lb
h	altitude, ft
I	moment of inertia, lb-ft^2
L	lift, lb
l	length, ft
M	Mach number
q	dynamic pressure, lb/ft^2
S	reference area, ft^2
t	thickness
V	velocity, knots
W	weight, lb
Δ	increment
Λ	sweep angle
Subscripts:	
app	approach
i	induced
lei	leading-edge inboard
leo	leading-edge outboard
o	zero lift
ref	reference
tei	trailing-edge inboard
teo	trailing-edge outboard
w	wave
x	longitudinal axis
y	spanwise axis
z	transverse axis
Abbreviations:	
a.c.	aerodynamic center
app	approach
AR	aspect ratio
CDM	Configuration Definition Module
c.g.	center of gravity
EIS	entry into service
FAR	Federal Aviation Regulations
FLOPS	Flight Optimization System
FS	fuselage station, ft
HSCT	high-speed civil transport
HSR	High-Speed Research
LE	leading edge
MAC	mean aerodynamic chord
SFC	specific fuel consumption, (lb/hr)/lb
TBE	turbine bypass engine
TDF	time, distance, and fuel
TE	trailing edge
TOFL	takeoff field length, ft
TOGW	takeoff gross weight, lb
XLEI	x-coordinate of inboard leading edge
XLEO	x-coordinate of outboard leading edge
XTEI	x-coordinate of inboard trailing edge
XTEO	x-coordinate of outboard trailing edge
YI	y-coordinate of inboard side
YMAC	spanwise location of MAC
YO	y-coordinate of outboard side

Design Concept and Description

A three-view drawing of the baseline Mach 2.4 configuration is shown in figure 1. The wing planform was developed for good supersonic cruise performance while still maintaining adequate low-speed characteristics. A detailed layout of the wing planform is shown in figure 2. A parametric study, the results of which are presented in appendix A, was conducted and led to the selection of this planform. The study showed that the high-speed penalty for reducing inboard wing panel leading-edge sweep was significant and would compromise high-speed performance. This was not true for outboard sweep and outboard panel aspect ratio. A low-sweep, high aspect ratio outboard panel resulted in relatively small penalties and projected improved low-speed characteristics. A second, more detailed study was then conducted to refine the planform; however, the results showed no improvement in the modified planforms (see appendix B). A sizing study of an earlier configuration led to the selection of a wing area of 9100 ft^2. It will be shown in a later section that this wing area leads to an acceptable baseline configuration.

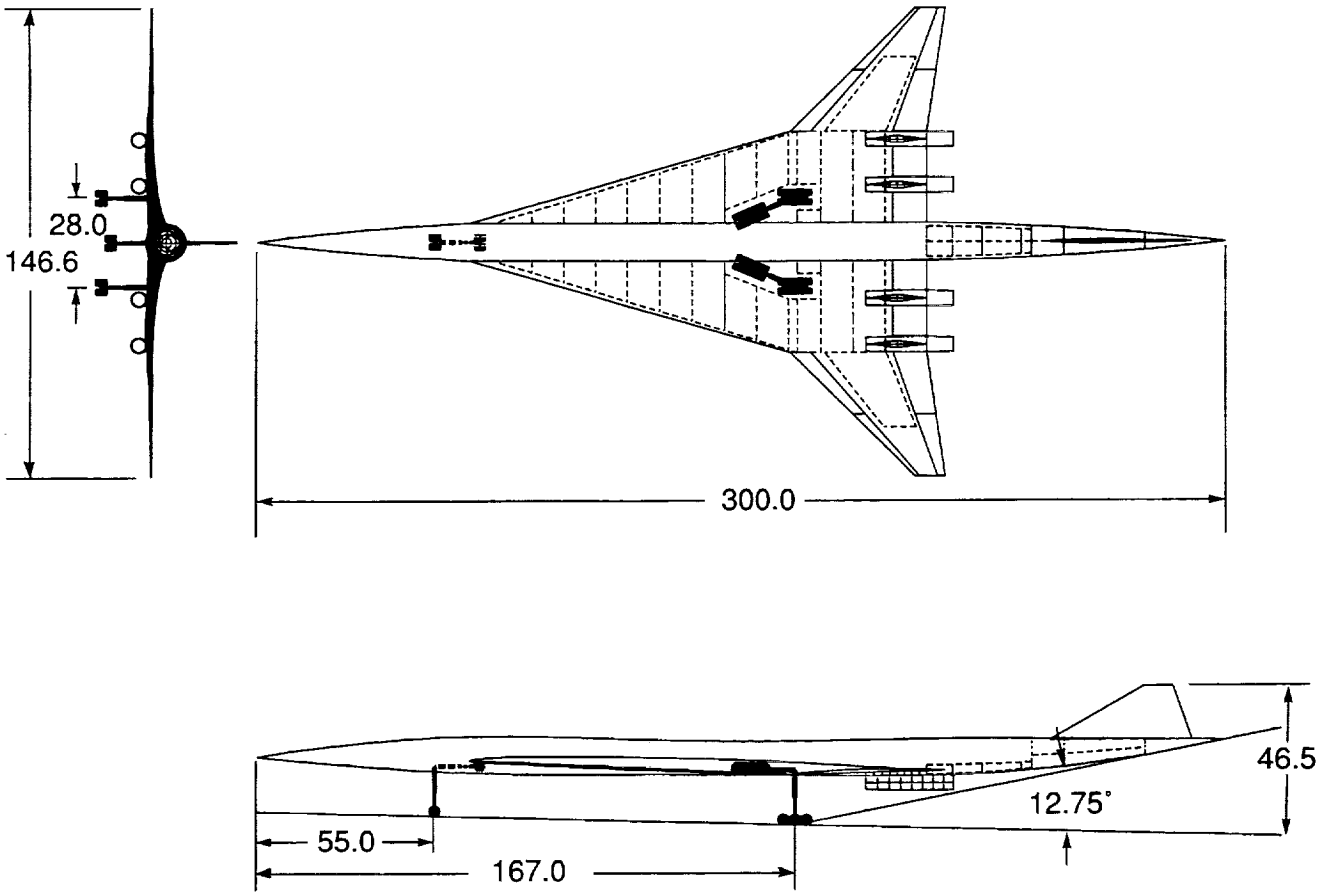

Figure 1. Three-view drawing of Mach 2.4 configuration. Linear dimensions in feet.

At Mach 2.4, the inboard leading-edge sweep of 74° yields a subsonic Mach number (0.66) normal to the leading edge while providing sufficient lifting length (length over which the lift is distributed) to lower the wave drag due to lift (inversely proportional to the lifting length squared). The 45° swept outboard panel has a relatively high aspect ratio of 3 to increase span, thus reducing induced drag (inversely proportional to the span squared). The apex of the wing leading edge projected to the centerline is located 45 ft aft of the nose of the configuration (FS 45). The wing incorporates an NACA 64A-series airfoil thickness distribution that was modified, as shown in figure 3, to increase the structural depth at the rear spar. The thickness-to-chord ratio varies linearly from 3 percent at the wing root to 2.5 percent at the break and is constant from there to the tip. The spanwise thickness distribution was selected based on a compromise between reduced wave drag and increased fuel volume.

Fifteen-percent-chord leading-edge flaps are located on the outboard panel only, while the trailing-edge flaps are 25 percent chord on the outboard panel and a constant chord of 10.6 ft on the inboard panel. The highly swept inboard panel has a low Mach number normal to the leading edge, which results in an insensitivity to leading-edge camber and allows effective low-speed performance without leading-edge devices. The exclusion of inboard leading-edge flaps also yielded a lower overall wing weight and left more wing volume for fuel.

A diagram of the interior layout of the fuselage is illustrated in figure 4. The configuration utilizes a synthetic vision system in the cockpit that has the capability of displaying both visible displays (e.g., television views from more than one location on the aircraft) and nonvisible displays such as radar and infrared for enhanced safety at night and in inclement weather. Ground-handling visibility should also be improved with multiple camera locations. The flight deck has provision for a pilot and copilot in a side-by-side arrangement. The main cabin will seat 251 passengers in rows of 4 or 5 seats abreast at 34 in. pitch with a single aisle. Two main entrances are

	1	2	Total
Wing area, ft 2	7098	2002	9100
Aspect ratio	0.673633	2.99997	2.36319
Taper ratio	0.259994	0.219614	0.0570983
LE sweep, deg	74	45	
TE sweep, deg	0	8.35365	
Span, ft	69.148	77.498	146.646
Root chord, ft	162.936	42.3625	
Tip chord, ft	42.3625	9.30339	
MAC, ft	114.452	29.3585	95.7312
YMAC, ft	13.9027	15.2422	21.8037
Length, ft			168.626

No.	Trapezoidal coordinates, ft					
	XLEI	XTEI	YI	XLEO	XTEO	YO
1	0	162.936	0	120.574	162.936	-34.574
2	120.574	162.936	-34.574	159.323	168.626	-73.323
3	20.9245	162.936	6	120.574	162.936	34.574
4	152.345	162.936	6	152.345	162.936	15.287
5	152.345	162.936	20.287	152.345	162.936	29.574
6	126.928	152.345	34.574	160.719	166.300	73.323
7	120.574	126.928	34.574	139.949	143.824	53.949
8	139.949	143.824	53.949	159.323	160.719	73.323
9	152.345	162.936	34.574	159.323	165.781	53.949
10	159.323	165.781	53.949	166.300	168.626	73.323

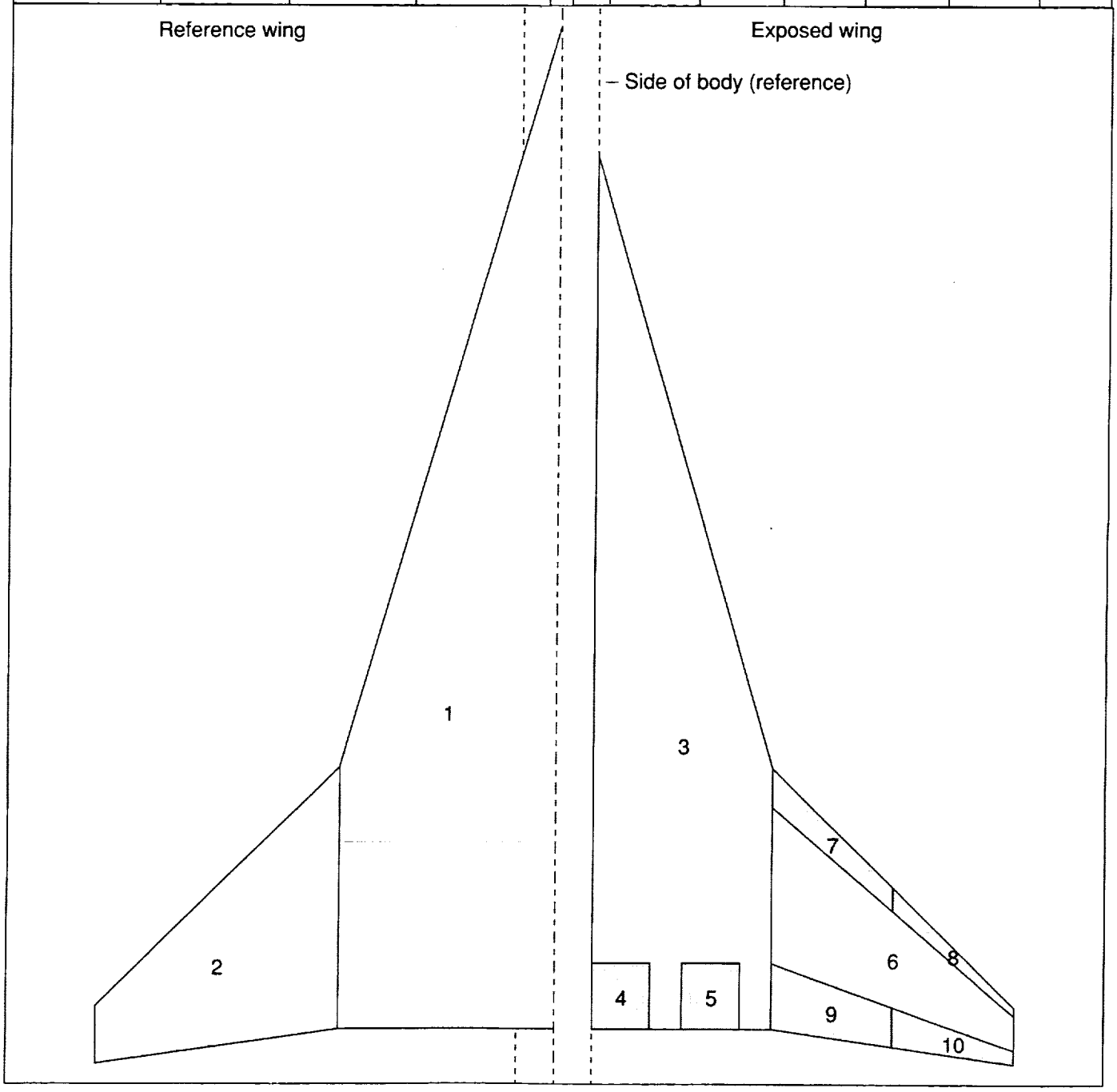

Figure 2. Configuration wing planform definition.

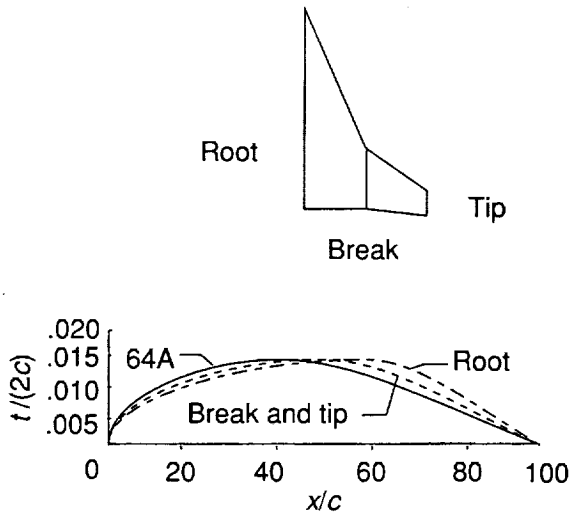

Figure 3. Comparison of airfoil thickness distributions at a maximum t/c of 0.03.

located on each side, forward of the first row of seats and aft between the last row of seats and the aft lavatories. Eight emergency exits are provided, four along each side between the forward and aft entrance doors. There are six lavatories, two forward and four aft. There are two galleys in the configuration, a small one adjacent to the front entrance and a larger one in the aft portion of the cabin behind the aft lavatories. This interior layout was selected to position most of the passengers ahead of the engine nozzles to increase passenger comfort. The present configuration has no windows, which yielded the simplest and lowest weight structure and also simplifies interior environmental control. Exterior visibility is supplied by television screens in the seat backs. These screens could also be used for entertainment or to disseminate information such as connecting flight gate information and updated arrival times.

Four engines are mounted on the underside of the wing in separate axisymmetric nacelles. The underwing placement allows for precompression of the airflow into the engine inlets; the longitudinal and spanwise nacelle locations were dictated by the wing planform, corresponding rear wing spar location, and inlet unstart considerations. Separate nacelles may reduce the effect an engine unstart could have on other engines and also enhance the safety aspects of the configuration in the case of a catastrophic

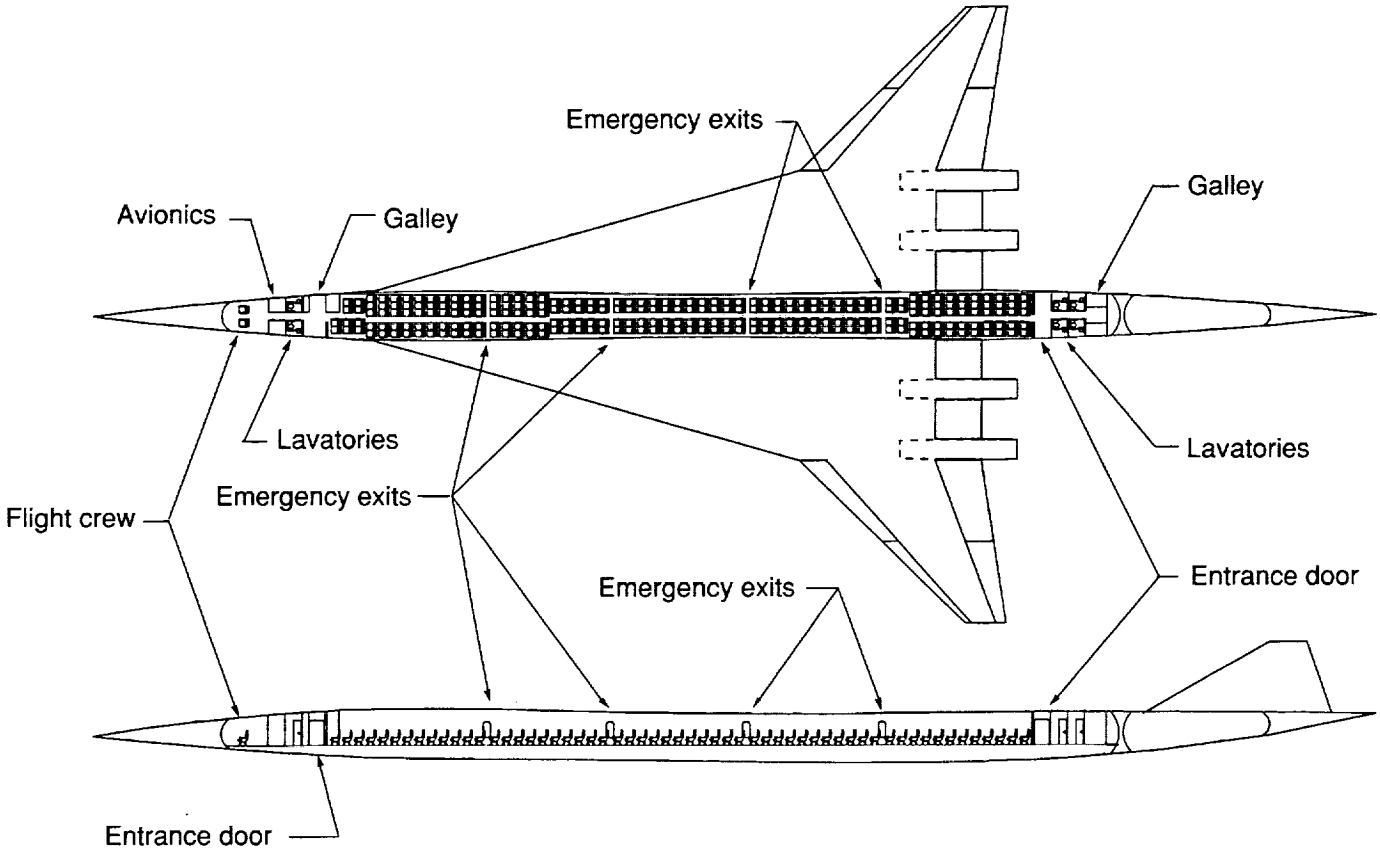

Figure 4. Interior layout.

	1
Wing area, ft^2	450
Aspect ratio	0.64279
Taper ratio	0.2
LE sweep, deg	60
TE sweep, deg	-18.8934
Span, ft	17.0075
Root chord, ft	44.0982
Tip chord, ft	8.81965
MAC, ft	30.3788
YMAC, ft	6.61402
Length, ft	44.0982

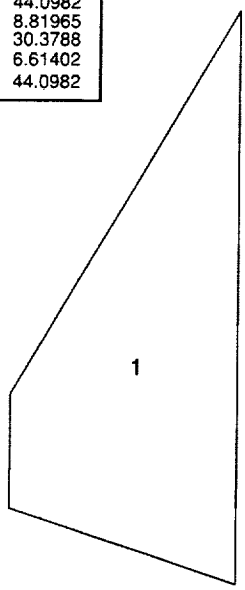

Figure 5. Vertical tail planform definition.

engine failure. Details of the propulsion system are discussed in a later section.

The main landing gear, a two-post arrangement with six wheels per post, is located at FS 167. These retract forward and inboard into the wing root with a small portion extending into the fuselage, below the passenger compartment. The nose gear, located at FS 55, retracts backward into the fuselage. The landing-gear system utilizes radial tires and carbon brakes for low weight.

Fuel is carried in 28 tanks in the wing and 3 tanks in the fuselage. The fuselage tanks, located in the aft portion of the fuselage behind and beneath the aft galley and passengers, provide critical fuel capacity and center-of-gravity control. Fuel tank locations are shown as dashed lines in figure 1.

A layout of the selected vertical tail planform is shown in figure 5. The leading edge of the root airfoil is 245.45 ft aft of and 5 ft above the nose of the configuration. An NACA 64A-series airfoil thickness distribution with a maximum thickness-to-chord ratio of 2.5 percent along the entire semispan was chosen based on structural and wave-drag considerations. A detailed tail sizing was not performed in this study; however, the tail volume coefficient of 0.032 was considered to be representative for a vehicle of this type.

Mass Properties

The aircraft weight, balance, and moments of inertias were estimated using the Flight Optimization System (FLOPS) discussed in reference 3. FLOPS employs empirical and semiempirical transport weight equations developed from a data base of transport aircraft with structures and subsystems weights based on conventional aluminum and titanium construction. Technology factors were used to modify the weights in FLOPS to reflect improvements related to advanced technologies, as listed in table I, and were obtained from various discipline experts at NASA Langley Research Center. Many of the weight reductions were due to utilization of advanced materials and construction techniques; however, the wing weight factor includes an additional improvement for the aeroelastic tailoring of the wing using composite materials. The inclusion of the benefits of fly-by-light and power-by-wire systems were reflected in the controls, hydraulics, electrical, air conditioning, anti-icing, and auxiliary power unit weight factors, which were developed by using reference 4. Advanced cockpit technology, including multipurpose displays, was responsible for the reductions in instrument and avionics weights. Configuration weights are presented in table II, and inertias are presented in table III.

The center-of-gravity envelope for the configuration is shown in figure 6(a) as a function of weight. The takeoff and landing weights for the design mission are indicated. This diagram was used to select a main landing gear location aft of the c.g. locations for the empty, operating, and zero-fuel weight conditions. Filling the forward fuel tanks first will be required to prevent accidental tip-back tail strikes. The c.g. location is managed throughout the flight by programming the fuel burn from the tanks and/or fuel pumping. During takeoff and landing, the c.g. location will be positioned just forward of the main landing gear to minimize the control power required for rotation while providing sufficient weight on the nose gear for ground operations. The c.g. position required for trim during the design mission is shown by the dashed line and was selected for minimum drag except at the takeoff and landing conditions. Figure 6(b) shows the variation of c.g. and aerodynamic center locations with Mach number. At low subsonic Mach numbers the trailing-edge flaps are deflected down for improved aerodynamic efficiency. The c.g. location required to trim the nose-down moment caused by the flap deflection is aft of the aerodynamic center, which results in a 4-percent

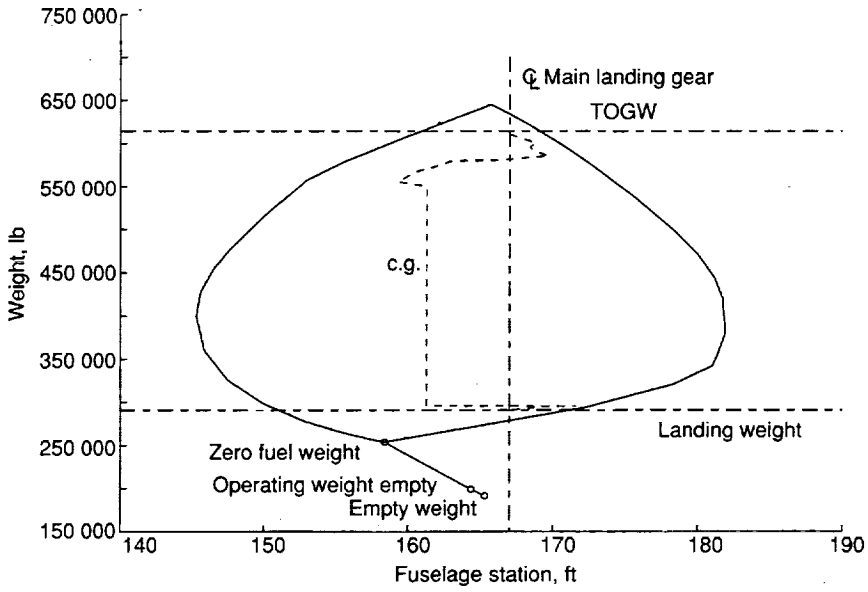

(a) Center-of-gravity envelope.

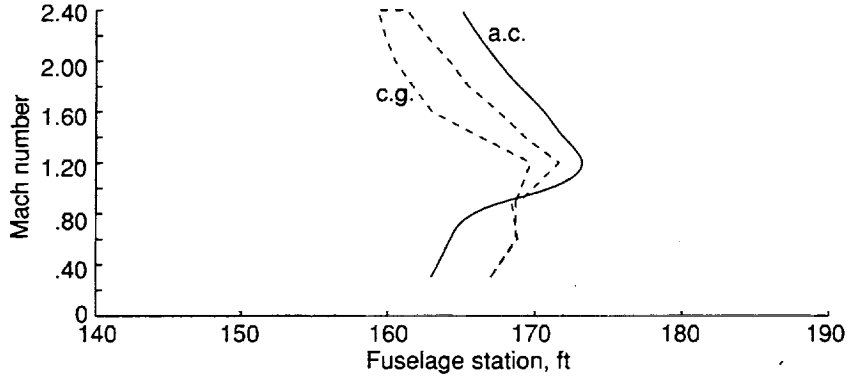

(b) Variation of center of gravity and aerodynamic center with Mach number.

Figure 6. Center-of-gravity plots.

statically unstable configuration. As Mach number increases through the transonic region, less flap deflection is required for minimum drag. The c.g. position required for trim then moves ahead of the aerodynamic center (a.c.) and the configuration becomes statically stable at approximately Mach 0.9. At supersonic speeds, the flaps are undeflected and the static margin is maintained between 4 percent and 8 percent stable. It should be noted that the positive stability level is due to the positive zero-lift pitching moment inherent in the wing design and has no trim drag penalty associated with it. Although a detailed investigation of the dynamic characteristics of this configuration was beyond the scope of the current study, it is believed that a digital control system can be designed to provide sufficient dynamic stability throughout the flight envelope.

Aerodynamics

Zero-Lift Drag

The zero-lift drag for the clean configuration is shown as a function of Mach number in figure 7 for representative subsonic and supersonic flight altitudes of 30 000 ft and 60 000 ft, respectively. Zero-lift drag consists of skin-friction drag, form drag, roughness drag, and volume-wave drag. Skin-friction drag was calculated using the T' method of Sommer and Short (ref. 5). Form drag was calculated with the geometry-dependent factors of the method of reference 6, and roughness drag was calculated empirically as a percentage of skin friction. Zero-lift wave drag was calculated with the Configuration Development Module (CDM) of reference 7.

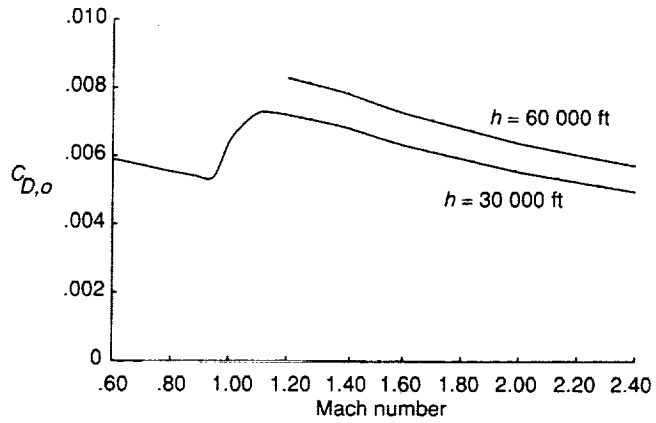

Figure 7. $C_{D,o}$ characteristics.

The wave-drag evaluation program has the ability to define a minimum wave-drag fuselage in the presence of the remaining aircraft components at a given Mach number. This feature was used to optimize the fuselage under the constraint of a minimum cabin radius that could accommodate four-abreast seating. The average-equivalent-body area distributions of the various configuration components are shown in figure 8.

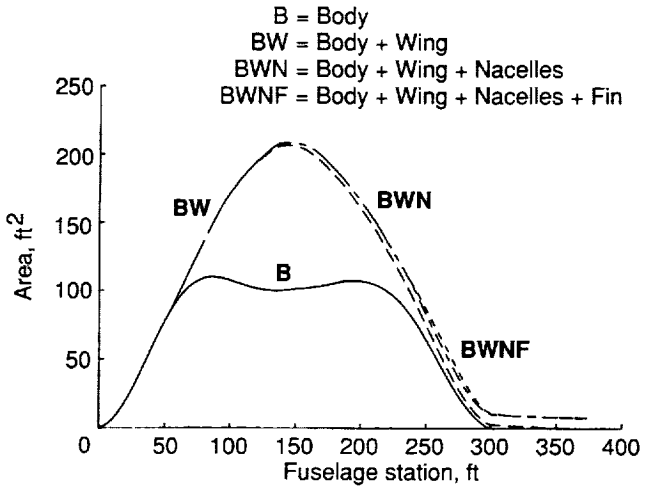

Figure 8. Average-equivalent-body area distribution at Mach 2.4.

Landing-gear drag was estimated based on unpublished data for a similar configuration scaled to match the frontal area of the struts and tires at an angle of attack of 0°. This value was used at all angles of attack.

Lift-Dependent Drag

The camber and twist of the wing were optimized for supersonic cruise with the modified linear-theory method of reference 8, which takes into account the effect of leading-edge thrust and vortex lift. Recommendations for supersonic wing design, documented in reference 9, were also applied to the optimization process. The effect of wing-nacelle interference on this configuration is negligible because of the extremely small change in cross-sectional area of the nacelles. A comparison of the cruise drag of wings with this planform, designed by using references 10 and 11, both with and without nacelle interactions showed less than a one-half count difference at cruise. It was, therefore, decided that for this particular configuration wing-nacelle interference effect would not be included. Figure 9 shows the resulting supersonic drag-due-to-lift polars at Mach numbers of 1.2, 1.6, 2.0, and 2.4. The supersonic drag due to lift, angle of attack versus lift coefficient, and static-longitudinal stability characteristics were estimated by using these same methods. The supersonic total drag polars are shown in figure 10 for a representative supersonic cruise altitude of 60 000 ft.

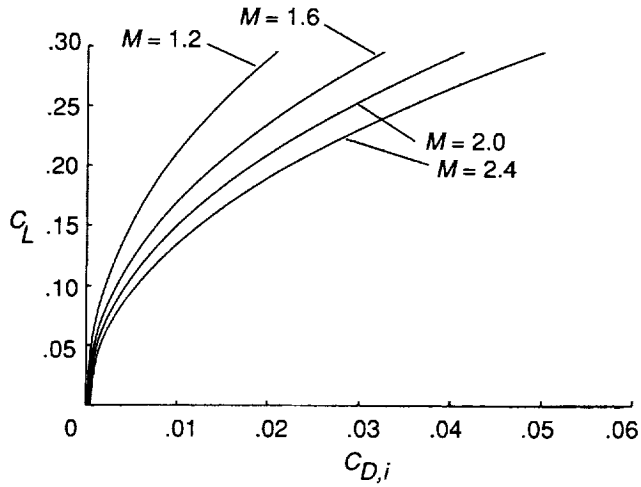

Figure 9. Supersonic drag due to lift.

The method of reference 12 was used to determine the subsonic drag polars. This method also takes into account the effects of leading-edge thrust and vortex lift. Leading- and trailing-edge flaps were deflected to minimize drag with the c.g. required for trim constrained to be forward of FS 169 for stability reasons. Figure 11 shows the resulting total-drag polars at subsonic Mach numbers of 0.6, 0.8, and 0.9 at a representative altitude of 30 000 ft. Transonic drag polars were developed by using an empirical method in conjunction with the previously developed supersonic and subsonic polars.

Takeoff and landing drag polars were developed with the methods of references 8 and 12. Leading- and trailing-edge flap settings for best performance

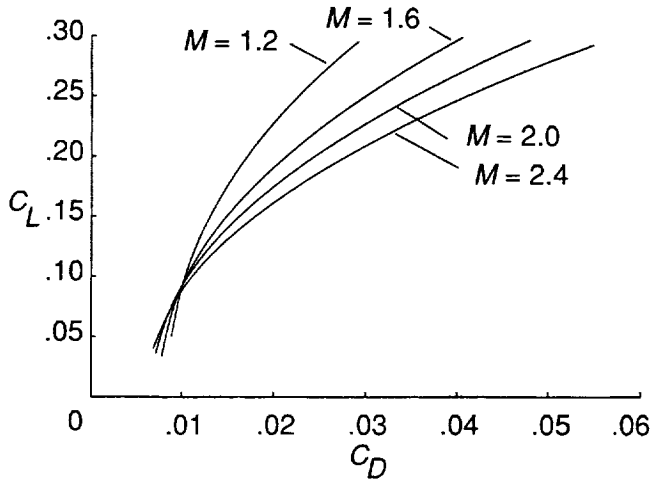

Figure 10. Supersonic total-drag polars. h = 60 000 ft.

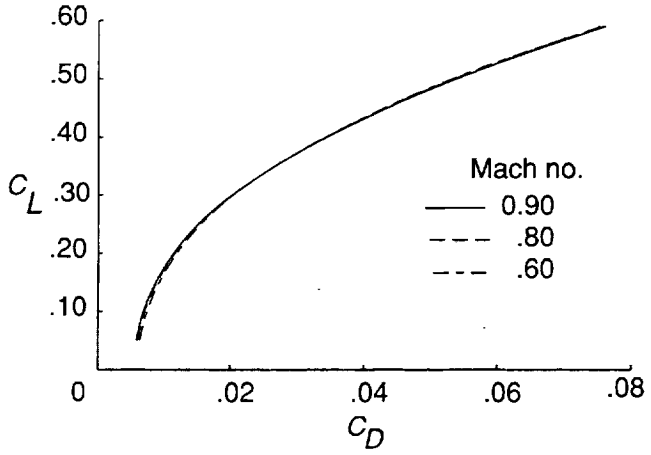

Figure 11. Subsonic total-drag polars. h = 30 000 ft.

were initially developed from the method of reference 8 to determine an optimum camber surface for the required takeoff and landing lift coefficients on "restricted areas" of the wing representing the flap locations. From those results, actual leading- and trailing-edge flap deflections with respect to supersonic cruise shape versus span were chosen, and a matrix of leading- and trailing-edge flap multipliers were used to develop a family of drag polars that are trimmed for a c.g. location of FS 167. The leading-edge flaps will be varied during takeoff and held constant during landing, while the trailing-edge flaps will be used for trim and control throughout the flight. The takeoff and landing polars are shown in figure 12, and the corresponding flap schedules are shown in figures 13 and 14.

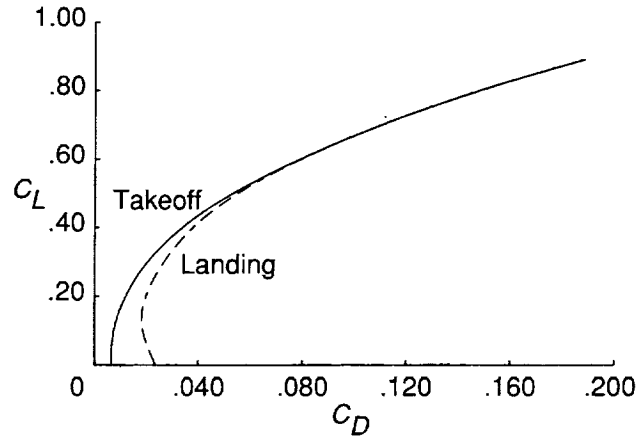

Figure 12. Trimmed takeoff and landing polars. M = 0.3; sea level. $C_{D,\text{landing gear}}$ = 0.0082 not included in polars.

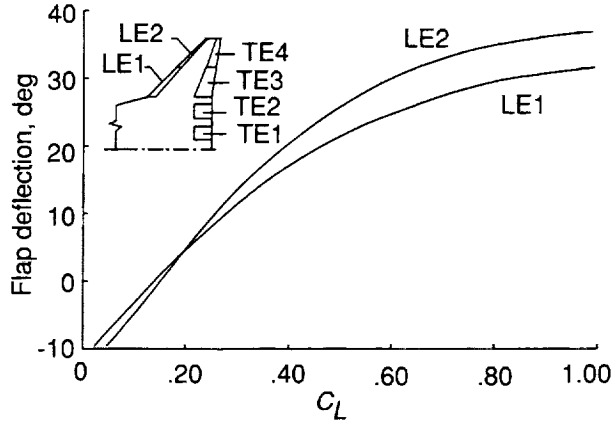

(a) Leading-edge flaps.

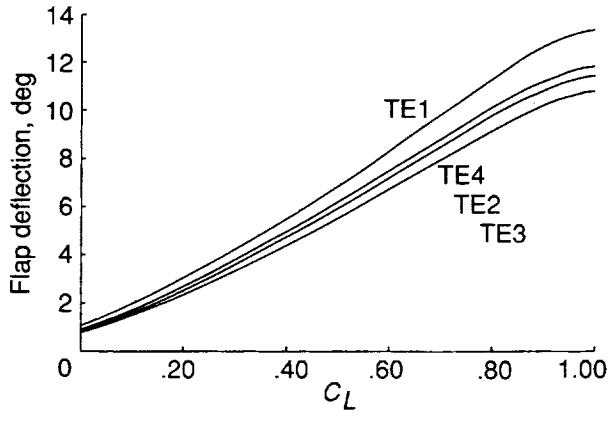

(b) Trailing-edge flaps.

Figure 13. Programmed flap schedules for takeoff. Flap deflections measured streamwise.

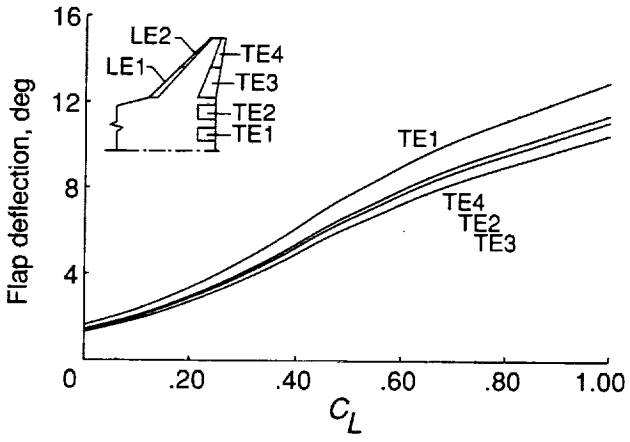

Figure 14. Programmed flap schedules for landing. Flap deflections measured streamwise. LE1 = 27.7°; LE2 = 33.6°.

Maximum Lift-Drag Ratio

The maximum trimmed lift-drag ratio versus Mach number is shown in figure 15 at representative altitudes of 30 000 ft and 60 000 ft for subsonic and supersonic cruise conditions. The values vary from $(L/D)_{max} = 17.6$ at a Mach number of 0.90 to $(L/D)_{max} = 9.0$ at the Mach 2.4 design condition.

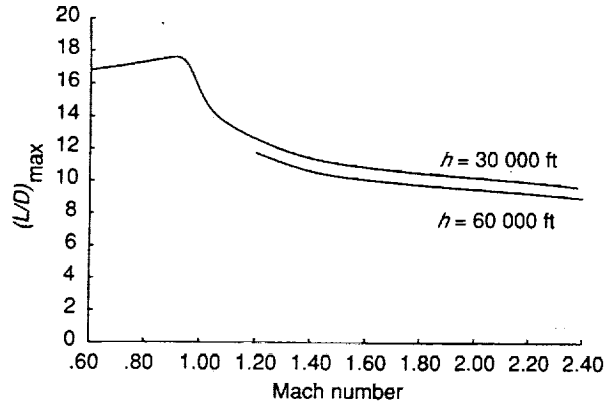

Figure 15. Maximum lift-drag ratios.

Propulsion

The baseline engine is a NASA-defined nonafterburning turbine bypass engine (TBE). The TBE is essentially a turbojet with a valve that allows compressor discharge air to bypass the primary burner and the turbines. As the engine power is reduced, the amount of bypass air decreases, thus allowing the inlet airflow to remain constant, resulting in reduced spillage and boattail drag. The overall pressure ratio, dictated by the maximum allowable compressor exit temperature, maximum turbine inlet temperature, and propulsion system weight (ref. 13) are consistent with an aggressive application of technology for the year 2005 EIS. Customer bleed and power extraction per engine are 1.0 lb/sec and 200 hp, respectively. The U.S. Navy/NASA Engine Program (refs. 14 and 15) combined with an installation module based on reference 16 was used to predict installed propulsion system performance. Figures 16 and 17 show the propulsion system standard day performance characteristics, including inlet spillage and nozzle boattail drag, for various altitudes. The inlet is an axisymmetric, mixed compression, translating centerbody inlet and the nozzle is an axisymmetric, mixer ejector nozzle designed to entrain external air during takeoff to reduce unsuppressed takeoff noise by 20 dB. Achieving this level of suppression while maintaining a high cruise gross thrust coefficient of 0.985 will be a challenge. The scaled nacelle and engine geometry is shown in figure 18.

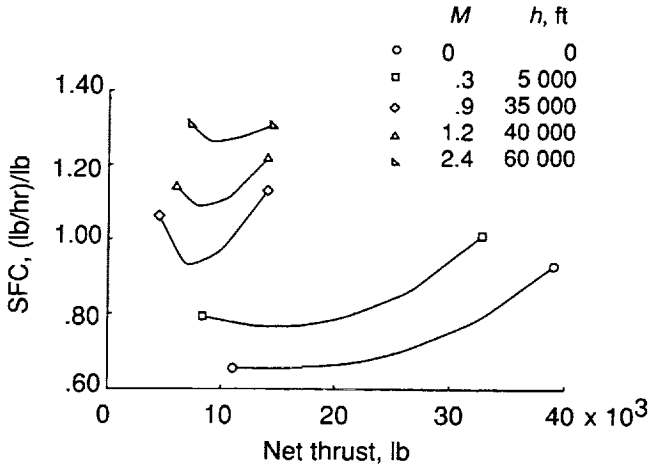

Figure 16. Engine SFC as a function of thrust.

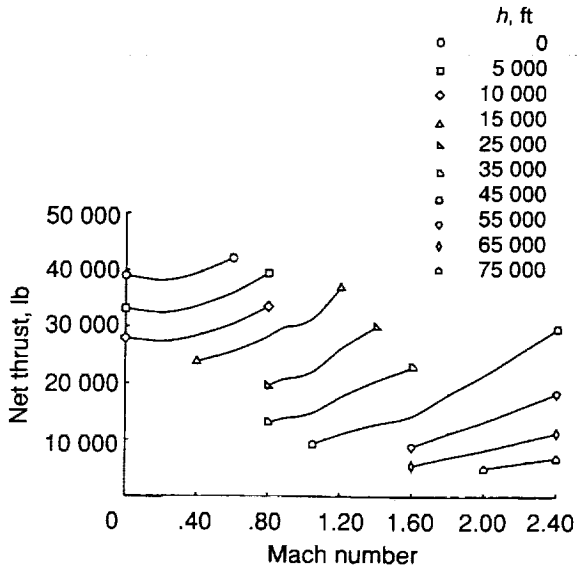

Figure 17. Engine thrust as a function of Mach number.

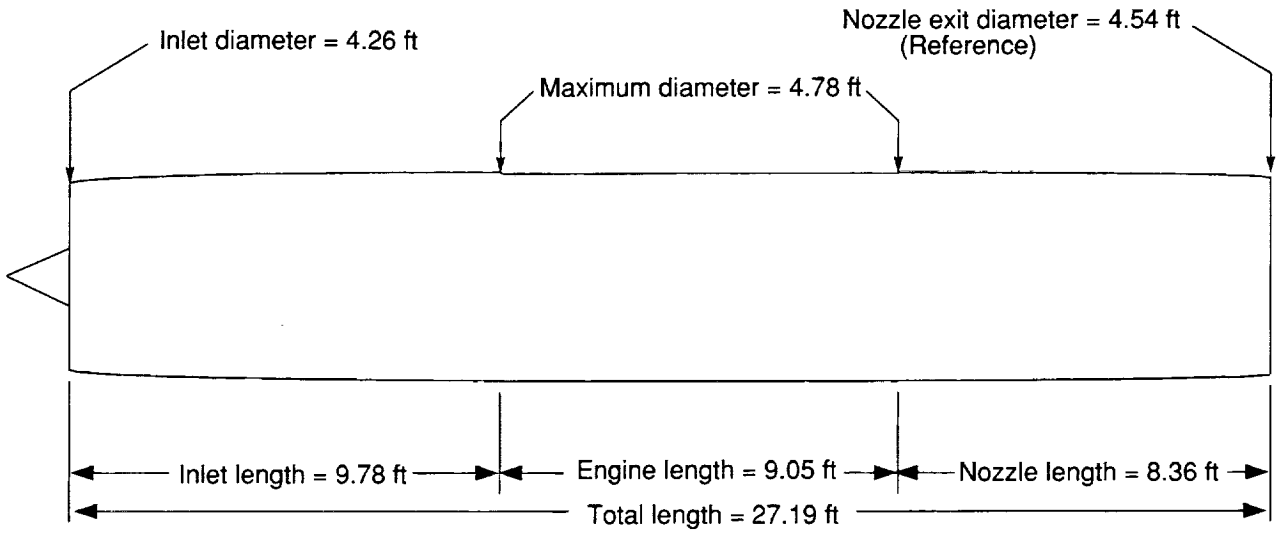

Figure 18. NASA Mach 2.4 TBE nacelle and engine geometry scaled for 39 000 lb installed net thrust (takeoff).

Performance and Sizing

The estimated vehicle performance and the results of sizing the wing area and engine thrust for minimum TOGW are presented in this section. Schematics of the design mission profile and reserve mission are shown in figure 19. A mission summary for the configuration is given in table IV. This mission includes:

A. Fuel for 10 min warm-up and taxi out at idle power

B. Actual fuel usage for takeoff to start of climb

C. Time, distance, and fuel (TDF) for actual climb (minimum fuel to climb path)

D. TDF for cruise at best altitude at M = 2.4

E. TDF for actual descent at maximum L/D, idle fuel flow

F. Reserve fuel allowance (no range credit) including:

1. Missed approach
2. Climb to reserve cruise condition
3. Cruise at Mach 0.9 and best altitude for 250 n.mi., including climb and descent
4. Hold for 30 min at Mach 0.6 and best altitude for minimum fuel flow
5. Descent from hold condition at maximum L/D ratio, zero thrust
6. Additional fuel reserve allowance: 5 percent of trip fuel (C, D, and E above)

G. No time, fuel or distance credit or penalty for approach, landing, or taxi in

Figure 20 shows a sizing "thumbprint" for this configuration. All the potential solutions represented in this design space will meet the 6500-n.mi. range requirement. Constraint lines for takeoff field length, excess fuel volume, and approach velocity define the limits of a feasible configuration. The minimum TOGW configuration is constrained by takeoff field length and mission fuel volume and has a TOGW of 609 000 lb, wing area of 8400 ft^2, and 41 500-lb-thrust engines. Experience has shown that because of approximations in the sizing equations, it would be difficult to develop a detailed configuration with these characteristics. The fuel-volume equations used in the sizing process do not properly scale the volume in the wing that is unusable for fuel such as that reserved for landing gear or insulation and, as a result, overpredicts the amount of fuel volume in wings smaller than the baseline. As seen in figure 6, not all the fuel volume is usable because of trim considerations. The actual fuel volume limit would be much closer to the original baseline configuration. Further, only a small reduction in TOGW, less than 5000 lb, could be achieved by changing the wing area and engine size. Resizing to the minimum weight configuration would also eliminate flexibility in c.g. location at takeoff. Having some flexibility in c.g. location with the slightly larger vehicle may be useful in solving problems such as community noise constraints. Thus, the original configuration with a wing area of 9100 ft^2 and engines sized to 39 000 lb thrust each was selected as the baseline.

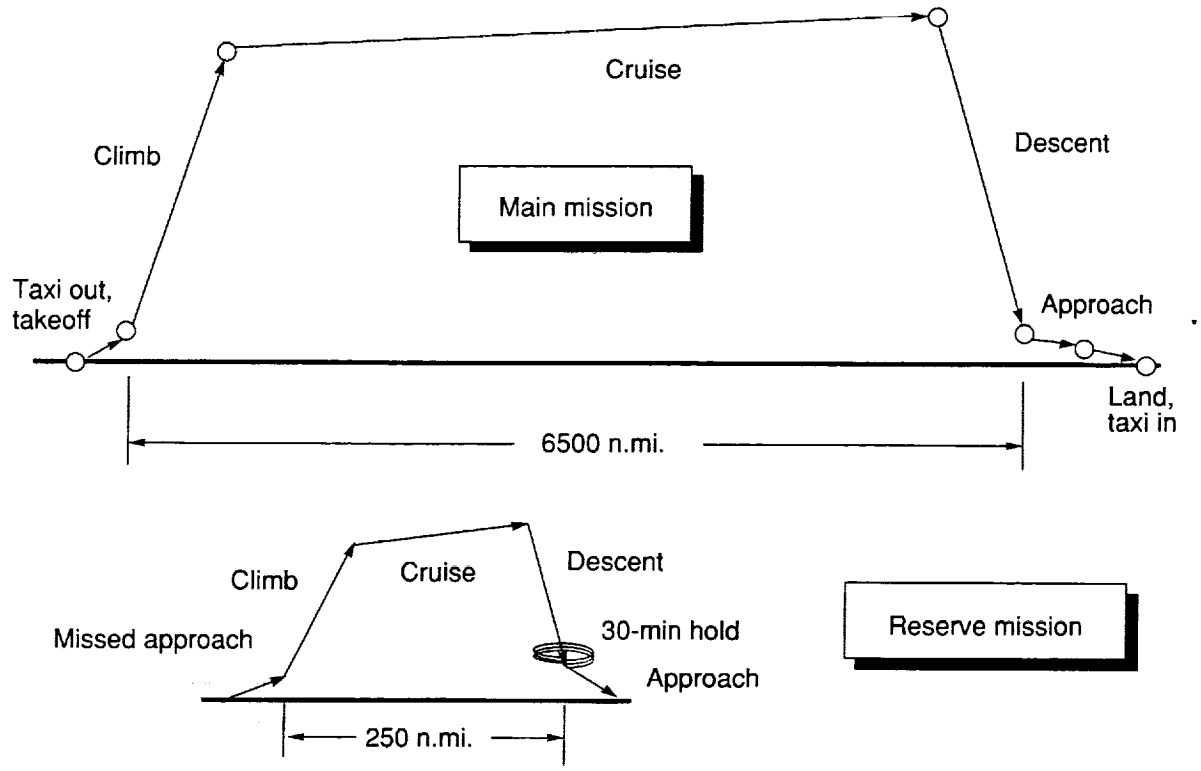

Figure 19. Design mission profile and reserves.

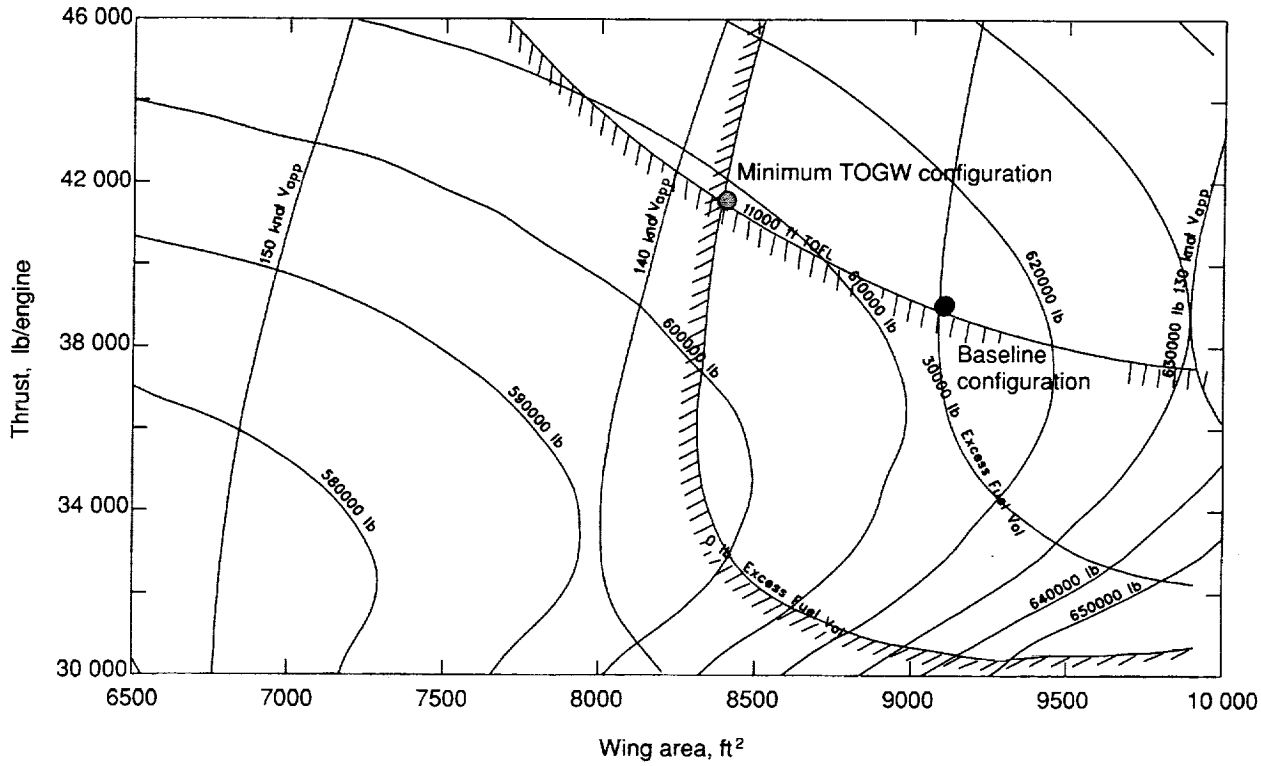

Figure 20. Sizing diagram for Mach 2.4 baseline configuration.

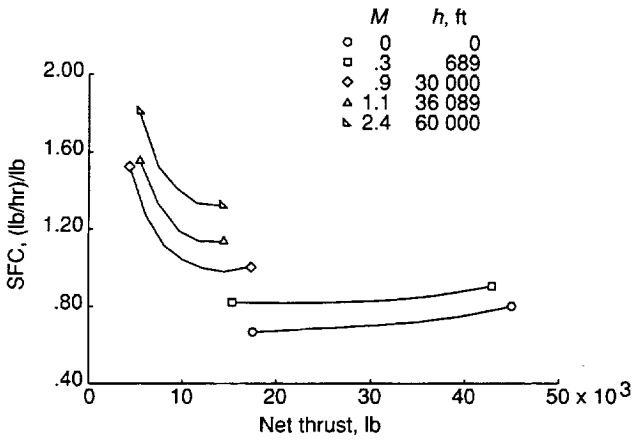

Figure 21. Alternate engine SFC as a function of thrust.

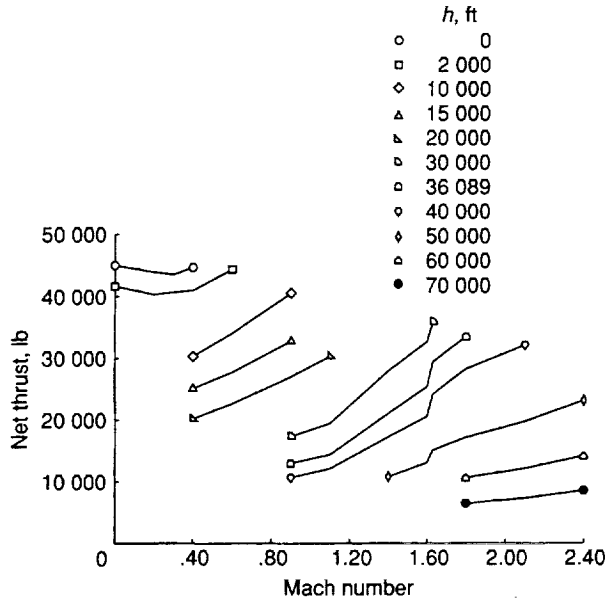

Figure 22. Alternate engine thrust as a function of Mach number.

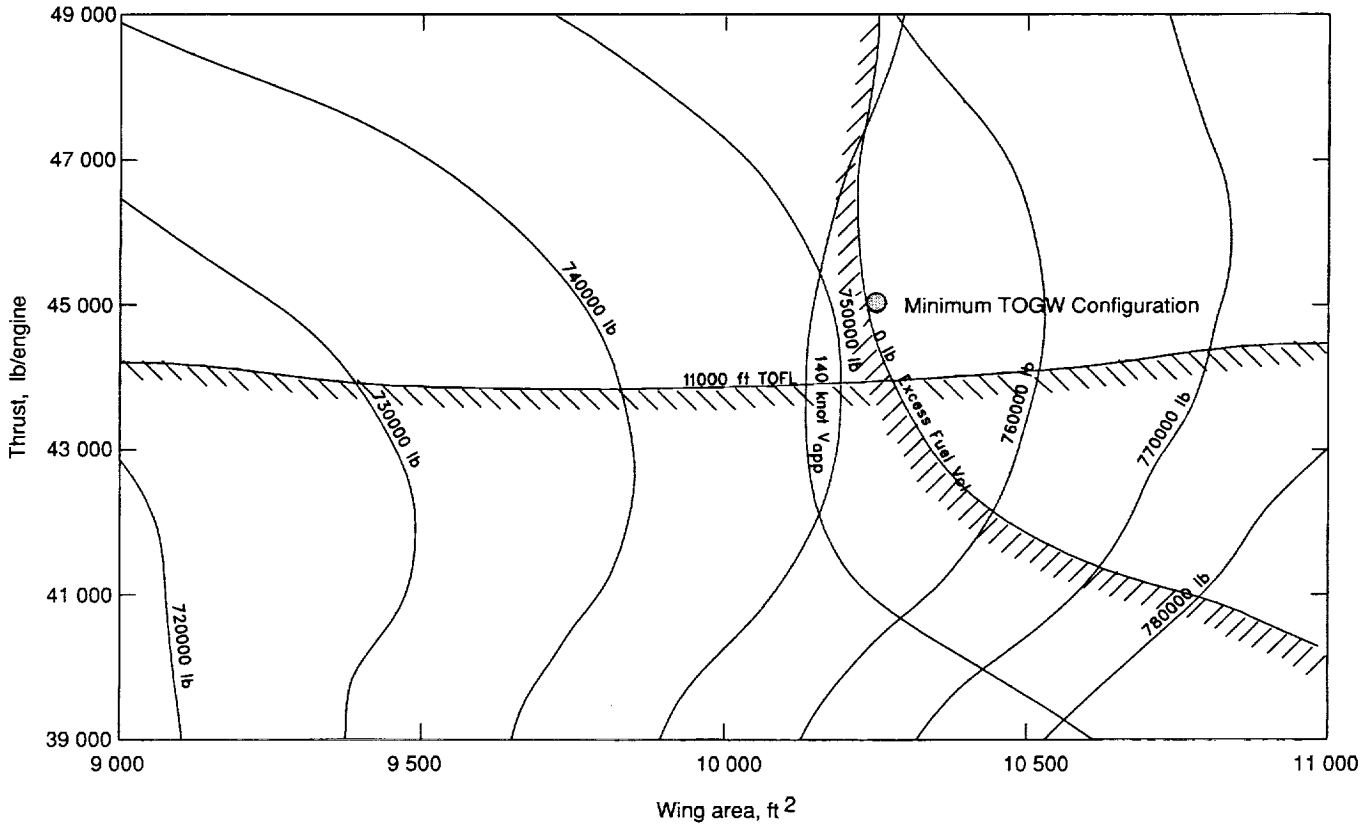

Figure 23. Sizing diagram for Mach 2.4 configuration with alternate engines.

Resizing

This vehicle, as stated earlier, is a baseline to be used in evaluating the effects of technologies on a Mach 2.4 configuration. During the design cycle of this configuration, the propulsion experts in the HSR program had the opportunity to reevaluate the level of technology that would be available for a vehicle with an entry into service date of 2005. It was concluded that the original engines used for this baseline would not provide the service life required for commercial use. Therefore, an alternative engine has been designed to provide 9000-hr life for the hot rotating parts and 18 000-hr life for the rest of the engine. This requirement results in both an increase in weight and a decrease in efficiency. The standard day performance characteristics of this alternate engine are shown in figures 21 and 22. The effect of these alternate engines on the current design can be shown by resizing the configuration with the new engines installed. The greater fuel burn and heavier weights of these engines are the main reason for the increased vehicle weight. As shown in figure 23, both the wing area and engine thrust must increase to offset the poorer performing engines. The resized configuration has a wing area of 10 250 ft^2 and 45 000-lb-thrust engines. The 752 000-lb TOGW is an increase of approximately 138 000 lb as compared with the original configuration.

Concluding Remarks

A baseline Mach 2.4 high-speed civil transport configuration was developed as part of a family of baselines for technology integration studies in support of the NASA High-Speed Research Program. The details of the aerodynamic design, configuration layout, propulsion system integration, mass properties, mission performance, and sizing were presented.

The concept was designed to carry 251 passengers a distance of 6500 n.mi. with reserves. The configuration is unblended, with a relatively simple planform and four engines mounted in separate axisymmetric underwing nacelles. The uncomplicated layout was intended to facilitate system studies investigating the effects of application of advanced technologies to the baseline concept. The planform was designed to minimize supersonic drag due to lift and wave drag while maintaining good low-speed characteristics. The flap arrangement, full-span trailing edge and outboard only leading edge, was selected to minimize weight and complexity while providing adequate lift for takeoff and landing.

Advanced composite materials were used in conjunction with innovative structural designs to reduce weight. Systems integration, including synthetic vision for the cockpit and the use of electric actuators for the control surfaces, also helped to reduce weight. Weight factors that reflect these effects were developed with the help of discipline experts at NASA Langley Research Center and Lewis Research Center. These weight factors and a semiempirical weight estimation program were used to estimate weights, c.g. locations, and inertia data.

The propulsion system used in the study was a NASA-defined turbine bypass engine (TBE). The weight and performance predicted for the engine is dependent on aggressive development and application of advanced technologies in a variety of disciplines including materials, emissions, and acoustics. The successful development of a high-performance mixer ejector nozzle is critical for application of the TBE. Any substantial reduction in the predicted 20-dB suppression would require oversizing the engines to meet community noise regulations and severely impact the aircraft takeoff gross weight (TOGW).

The baseline configuration has a wing area of 9100 ft^2 and a TOGW of 614 300 lb. The four advanced turbine bypass engines have 39 000 lb thrust each and weigh 9950 lb each. The takeoff thrust-to-weight ratio and wing loading are 0.254 and 67.5 lb/ft^2, respectively. The configuration is sized by the 11 000-ft takeoff field length requirement and has an approach velocity of 134 knots.

A resizing of the baseline configuration using an engine that has the projected life for commercial use on a year 2005 entry-into-service vehicle was also performed. The resized configuration has a wing area of 10 250 ft^2 and 45 000-lb-thrust engines. The 752 000-lb TOGW is an increase of approximately 138 000 lb as compared with the original configuration.

NASA Langley Research Center
Hampton, VA 23681-0001
December 7, 1993

Table I. Technology Assessment Factors for Year 2005

Component	Weight factor
Wing[a]	0.70
Vertical	.80
Fuselage	.82
Nose gear	.85
Main gear	.75
Surface controls	.75
Hydraulics[b]	.03
Instruments[c]	.70
Electrical[b]	.95
Avionics[c]	.70
Furnishings	.85
Air conditioning[b]	.65
Anti-icing[b]	1.12
Auxiliary power[b]	.81

[a]Composites and aeroelastic tailoring.
[b]Fly-by-light, power-by-wire.
[c]Advanced cockpit technologies.

Table II. Mass and Balance Summary

Item	Percentage of W_{ref}	W, lb	Percentage of l_{ref}	Longitudinal c.g. location, in.
Wing	8.25	50 649	55.9	2014.0
Vertical tail	.29	1 758	90.5	3259.0
Fuselage	6.37	39 129	48.8	1757.0
Landing gear	2.34	14 397	51.3	1846.0
Structure total	**17.24**	**105 933**	**53.2**	**1916.9**
Engines/nacelles	6.48	39 803	67.7	2436.0
Miscellaneous systems	.15	918	61.4	2210.5
Fuel system tanks and plumbing	.75	4 579	66.1	2378.8
Propulsion total	**7.37**	**45 300**	**67.4**	**2425.7**
Surface controls	1.06	6 497	59.1	2127.8
Auxiliary power	.19	1 141	93.3	3360.0
Instruments	.17	1 049	29.9	1075.3
Hydraulics	.02	129	52.9	1902.6
Electrical	.75	4 615	32.8	1181.9
Avionics	.24	1 458	14.3	516.0
Furnishings and equipment	3.33	20 457	44.3	1593.2
Air conditioning	.72	4 441	51.4	1849.0
Anti-icing	.07	454	53.4	1922.3
Systems and equipment total	**6.55**	**40 241**	**46.2**	**1662.9**
Weight empty	**31.17**	**191 474**	**55.1**	**1983.9**
Flight crew and baggage (2)	0.07	450	11.7	420.0
Cabin crew and baggage (7)	.18	1 130	46.0	1655.0
Unusable fuel	.33	2 019	55.1	1982.2
Engine oil	.05	316	67.7	2436.0
Passenger service	.61	3 758	46.0	1655.0
Operating weight empty	**32.42**	**199 148**	**54.8**	**1973.0**
Passengers, 251	6.74	41 415	46.0	1655.0
Passenger baggage	1.80	11 044	46.0	1655.0
Miscellaneous items	.41	2 545	46.0	1655.0
Zero fuel weight	**41.37**	**254 152**	**52.9**	**1904.2**
Mission fuel and reserves	**58.63**	**360 150**	**55.1**	**1982.2**
Ramp (gross) weight	**100.00**	**614 302**	**54.2**	**1949.9**

Table III. Inertia Summary

Component (and related systems)	Weight, lb	Horizontal c.g.[a], in.	Lateral c.g.[a], in.	Vertical c.g.[a], in.	I, (lb-ft^2)/10^6, for— Roll[b] (I_X)	Pitch[b] (I_Y)	Yaw[b] (I_Z)	Product of inertia[c] (I_{XZ})
Fuselage	78 868	1676.0	0	12.0	2.830	507.347	507.347	−7.762
Wing + Carry-through	60 538	2009.5	0	−49.2	40.778	66.135	106.917	−.180
Vertical tail	2 520	3259.0	0	122.0	.037	.202	.165	3.509
Inboard nacelles	21 380	2436.0	225.2	−99.6	.041	.685	.685	−4.398
Outboard nacelles	21 380	2436.0	384.8	−99.6	.041	.685	.685	−4.398
Nose gear	1 700	660.0	0	−156.0	.028	.028	0	1.890
Main gear	12 762	2004.0	168.0	−150.0	.239	.239	0	−.249
Tank 1, per side	1 375	976.0	85.8	−20.8	.001	.012	.012	−.134
Tank 2, per side	3 892	1087.0	99.7	−27.1	.009	.035	.039	−.183
Tank 3, per side	6 922	1204.7	113.6	−32.8	.030	.064	.081	−.072
Tank 4, per side	10 205	1323.2	127.2	−37.3	.083	.107	.145	.121
Tank 5, per side	13 565	1442.5	140.4	−41.2	.155	.144	.236	.327
Tank 6, per side	16 881	1561.9	153.4	−44.2	.531	.177	.631	.464
Tank 7, per side	19 994	1681.4	166.3	−46.9	.828	.206	.955	.505
Tank 8, per side	13 980	1797.9	222.7	−53.2	.527	.141	.620	.326
Tank 9, per side	13 796	1932.8	269.0	−56.2	.506	.199	.676	.097
Tank 10, per side	3 473	2054.8	95.8	−46.1	.008	.018	.020	−.021
Tank 11, per side	7 604	2056.4	293.2	−55.9	.067	.038	.096	−.086
Tank 12, per side	20 290	2157.4	218.3	−52.1	1.399	.186	1.553	−.435
Tank 13, per side	13 244	2273.4	226.2	−52.4	.906	.117	1.013	−.479
Tank 14, per side	6 255	1781.5	516.7	−56.6	.282	.425	.706	.189
Tank 15	26 806	2938.1	0	9.7	.409	.429	.433	7.924
Tank 16	40 114	3123.4	0	20.2	.506	2.355	2.347	17.477
Tank 17	20 837	2669.3	0	−42.9	.165	1.803	1.943	−.819
Passengers and baggage	55 004	1652.5	0	0	.416	208.181	208.181	−4.335
Total aircraft (full fuel)	644 861	1979.7	0	−34.7	194.840	1942.361	2118.542	9.896
Total aircraft (no fuel)	254 152	1903.6	0	−32.1	81.215	980.903	1048.611	[d]−15.578

[a]c.g.'s are referenced to nose of configuration.
[b]Inertias are referenced to c.g. of each component.
[c]Inertias are referenced to total aircraft (full fuel) c.g.
[d]Inertias are referenced to total aircraft (no fuel) c.g.

Table IV. Mission Summary

Segment	Initial weight, lb	Fuel, lb		Time, min		Distance, n.mi.		Mach number		Altitude, ft	
		Segment	Total	Segment	Total	Segment	Total	Start	End	Start	End
Taxi out	614 302	1 933	1 933	10.0	10.0						
Takeoff	612 369	1 933	3 866	.8	10.8			0.300		0	
Climb	610 436	58 448	62 314	35.4	46.2	449.7	449.7	.300	2.400	0	57 002
Cruise	551 988	255 593	317 907	249.6	295.8	5729.7	6179.4	2.400	2.400	57 002	69 408
Descent	296 394	5 494	323 401	39.9	335.7	320.6	6500.0	2.400	.300	69 408	0
Reserves	290 901	36 749	360 150								
Taxi in		966		5.0	340.7						
Zero fuel	254 152										

Design range, n.mi.	6500.0
Flight time, min	324.9
Block time, hr	5.68
Block fuel, lb	324 368

Appendix A

Planform Trade Study I

The design of a high-speed civil transport requires a compromise between efficient high-speed performance and acceptable low-speed characteristics. These requirements tend to drive the wing planform selection in opposite directions, such as low leading-edge sweep for low-speed high-lift performance and higher sweep for supersonic cruise. The designer is, therefore, forced to choose a more complicated planform in order to have the flexibility to achieve a feasible compromise. As the number of design variables for the planform grows, the number of possible combinations becomes very large, increasing the effort required for optimization.

A trade study was conducted to select a planform for a Mach 2.4 configuration. A decision was made to use a planform consisting of two trapezoidal panels to limit the scope of the study to a manageable size. The design variables chosen were the leading-edge sweep of the inboard panel and the aspect ratio, area, and leading-edge sweep of the outboard panel. The taper ratio of the inboard panel was modified with panel area, while total wing area was held constant. These four planform design variables were thought to be the primary drivers between low-speed and high-speed performance. The trade study consisted of a matrix of three values of each of the four design variables, yielding 81 planforms for analysis. The endpoints of this matrix are shown in figure A1.

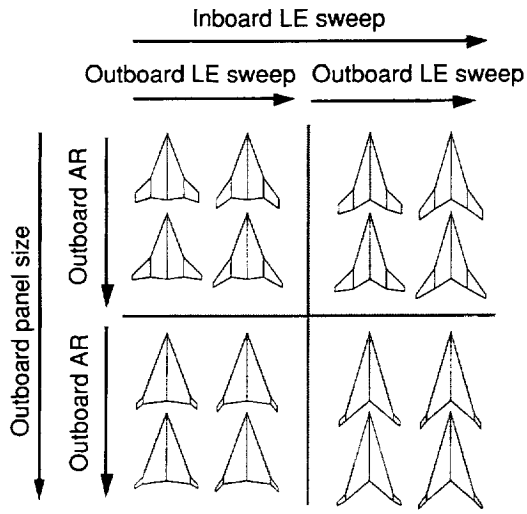

Figure A1. Matrix end points.

The primary goal of the analysis was to determine the corresponding trend in weight increments or drag increments due to changes in planform parameters to be used as guidelines in choosing a baseline planform. Those planform changes that had less of an effect on high-speed performance would be pushed toward the better low-speed value, while changes that had a harsher impact on high-speed performance would be chosen for optimum cruise benefits. The analysis data for all 81 planforms were reduced to trends for each design variable by condensing the slopes of the pertinent data to an overall result.

A total of 81 planforms were analyzed in this trade study. Each planform had a constant area of 11 500 ft^2, an initial estimate based on previous studies of planform area for this class of vehicle. The first planform variable was inboard leading-edge sweep with values of 70°, 72°, and 74°. Outboard leading-edge sweep was analyzed for values of 45°, 50°, and 55°. The aspect ratio of the outboard panel varied by 0.5 from 2.0 to 3.0. The outboard panel area was analyzed for values of 500 ft^2, 1500 ft^2, and 2750 ft^2. The values of these four planform parameters were chosen to correspond to planform layouts considered feasible, encompassing some extreme cases for high-speed or low-speed benefits.

The wing weight for each of the 81 planforms was calculated with the wing-weight equations from FLOPS. Wing weight is primarily dependent on planform shape, load path sweep, and flap area. For this study, the sweep of the load path was estimated to be equal to the sweep of the three-quarter chord of each panel. For the range of planforms investigated in this study, the weight increment due to flaps was assumed to be the same for all the planforms, so this increment was not calculated for the trend curves.

The drag due to lift at cruise conditions was calculated by the method of reference 8 for each planform studied. The camber distribution for each planform was optimized for cruise at a lift coefficient of 0.08 (an estimate of expected cruise C_L) and a Mach number of 2.4.

Wave-drag optimization was a more time intensive process than the above calculations. Thus, only the planforms with the 1500 ft^2 outboard panels were analyzed. Wings with constant 3-percent thickness-to-chord ratios were constructed in CDM. A generic fuselage with a constant volume of 23 000 ft^3 was optimized in the presence of each wing. The optimized fuselage was constrained to a minimum cross-sectional area of approximately 100 ft^2 in the cabin section. Wings were placed along the body such that the leading-edge break point remained in a constant longitudinal position. The zero-lift wave drag of each area-ruled wing-body combination was calculated at a Mach number of 2.4.

Increments in skin friction, form, and roughness drag were considered to be second order over the range of planform variables and were not calculated.

The sensitivity of wing weight to each of the design variables was estimated with FLOPS. The general trends, shown in figure A2, illustrate that as inboard leading-edge sweep increases, so does the wing weight. The only other significant effect on wing weight occurs for planforms with the small outboard panel. The other two design variables are shown to have a negligible effect on wing weight.

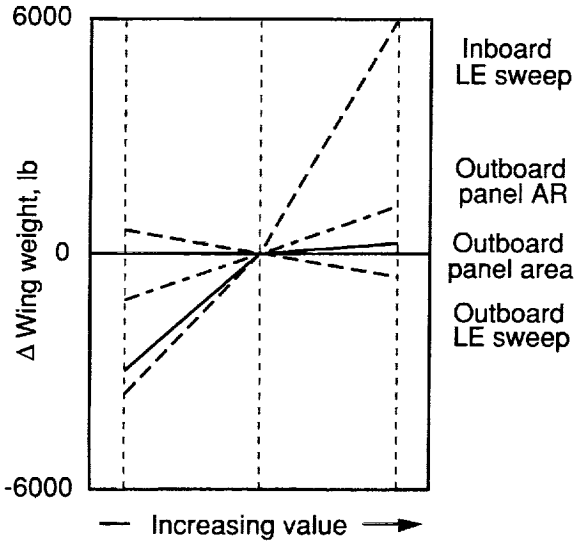

Figure A2. General weight trends.

The sensitivity of drag due to lift for each of the design variables was estimated and the general trends are shown in figure A3. As with wing weight, inboard leading-edge sweep has the largest effect on drag due to lift. The drag due to lift is shown to decrease with increasing sweep. Outboard panel size has a smaller impact on induced drag, with an induced drag reduction as the area is reduced. Again, outboard panel aspect ratio and sweep have much smaller effects on induced drag.

The sensitivity of wave drag to the design variables was estimated and is shown in figure A4. Zero-lift wave drag is shown to be dominated by inboard leading-edge sweep with much smaller changes due to outboard sweep and aspect ratio. The wave drag is shown to decrease with increasing leading-edge sweep.

Engineering judgment was used to rank the relative low-speed merits of each planform. Low-sweep, high-aspect-ratio outboard panels with sufficient chord lengths to incorporate leading- and

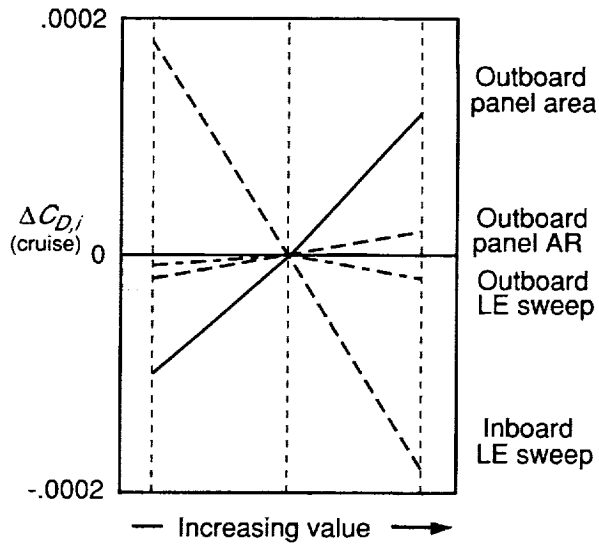

Figure A3. General drag-due-to-lift trends.

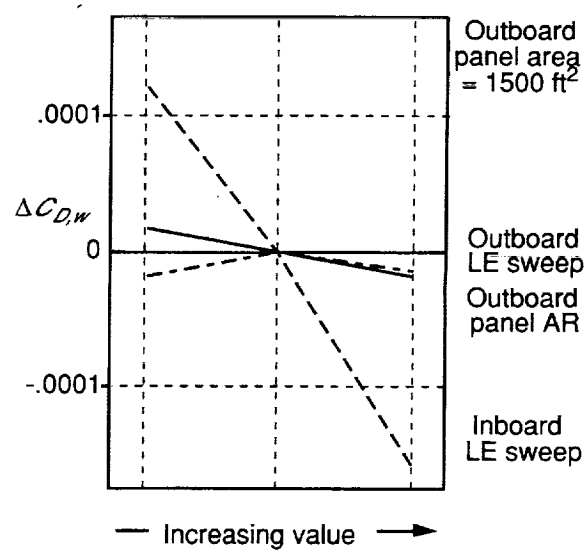

Figure A4. General wave-drag trends.

trailing-edge flap systems were considered desirable. The results of the study indicated that inboard leading-edge sweep was the dominant design variable. All the cruise drag components decreased with increased leading-edge sweep; however, wing weight increased with leading-edge sweep. This wing-weight penalty was due mainly to the increase in the sweep of the load path on the inboard portion of the wing. Because the load path typically tends to follow the rear wing spar, which is more a function of trailing-edge sweep than leading-edge sweep, the wing-weight result may be less than indicative. A more appropriate definition for sweep of the inboard load path in future studies would be to set it equal to the inboard trailing-edge sweep.

As a result of this trade study, a modified planform that had an inboard leading-edge sweep of 74° and an outboard leading-edge sweep of 45° was chosen. An inboard trailing-edge sweep of 0° was decided upon in an effort to reduce wing weight. A large outboard panel was chosen with an aspect ratio of 3.0, resulting in an outboard trailing-edge sweep of approximately 8.35°.

In conjunction with this planform trade study, a sizing study was done on an older HSCT configuration, the AST205 (ref. 17). The sizing study was based on the aerodynamics of the older configuration with the new engines to be used on the updated baseline. The results of this sizing study pointed to a planform area of 10 000 ft^2, a reduction in planform area of 1500 ft^2. The resulting baseline planform is shown in figure A5.

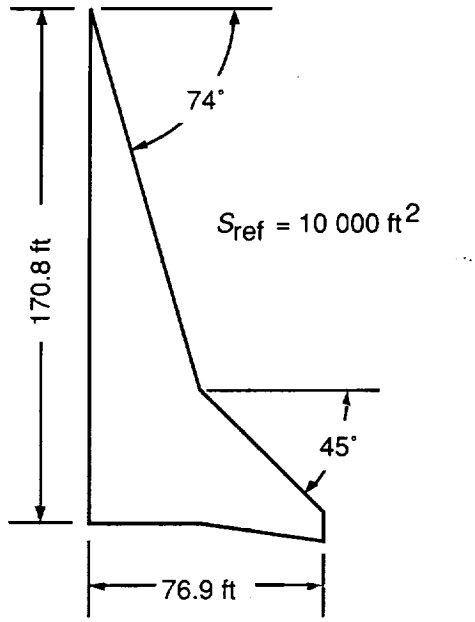

Figure A5. Resulting baseline planform.

The results of this study provided some basic guidelines for choosing an appropriate planform for a Mach 2.4 transport. The high-speed penalty for a reduced leading-edge sweep was significant and would compromise high-speed performance. However, the same is not true for outboard leading-edge sweep and outboard panel aspect ratio. A low-sweep and high-aspect-ratio panel did not result in relatively large penalties. The baseline planform chosen should provide good high-speed performance while maintaining acceptable low-speed characteristics.

Appendix B

Planform Trade Study II

The NASA Mach 2.4 baseline wing planform has 74° leading-edge sweep and 0° trailing-edge sweep on the inboard panel and 45° leading-edge sweep and 8.35° trailing-edge sweep on the outboard panel. This planform was chosen as a result of a previous planform trade study (see appendix A) and is shown in figure B1. The planform area was reduced from 10 000 ft^2 to 9100 ft^2, a result of sizing the baseline Mach 2.4 HSCT configuration.

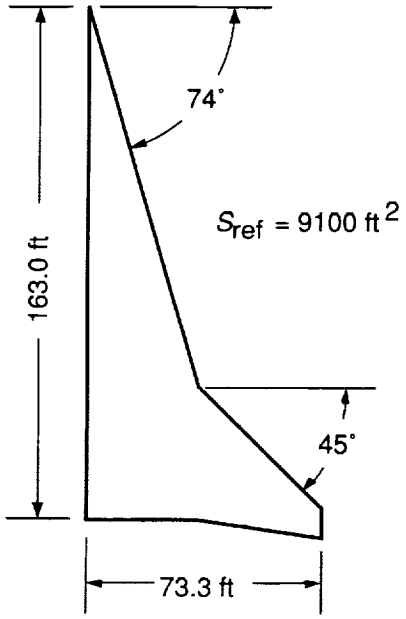

Figure B1. Baseline wing planform.

Concern over the high inboard leading-edge sweep of the baseline planform prompted a refinement study. In this study, the wing was again configured as two trapezoidal panels; however, new design variables were chosen to provide a clearer understanding of the trends. The planforms were defined by the leading- and trailing-edge sweep angles of the inboard and outboard panels, the span, the spanwise leading-edge break location, and the total area. Each of the four sweep angles was varied independently while holding the other design variables constant. It was felt that this approach better isolated the effects of these variables on wing performance and presented a set of design variables better suited to evaluating low-speed performance.

Takeoff gross weight (TOGW) was chosen as the figure of merit in comparing the various planforms in the refinement study. The FLOPS was used to determine the sensitivity of TOGW to incremental increases in drag and wing weight for the NASA Mach 2.4 baseline configuration. Each planform was then analyzed and the sensitivities were applied to the wing weight and drag of each to determine the TOGW increments.

Eight planform variations were analyzed in this study with each planform having a constant area of 9100 ft^2. Variations were derived from the current NASA Mach 2.4 baseline planform. The planform variations are shown in figure B2 and are broken down into isolated inboard and outboard leading- and trailing-edge sweep changes. Table BI gives the planform definitions.

Table BI. Planform Definitions

[Constants: S_{ref} = 9100 ft^2; $(b/2)_{inboard}$ = 34.6 ft; $(b/2)_{outboard}$ = 38.749 ft]

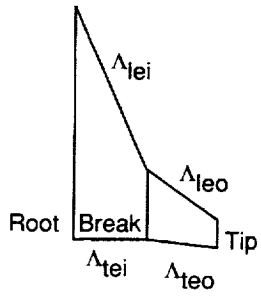

	1	2	3	4	5	6	7	8
Λ_{lei}, deg	74	72	70	74	74	74	74	74
Λ_{tei}, deg	0	0	0	0	−10	10	0	0
Λ_{leo}, deg	45	45	45	48	45	45	45	45
Λ_{teo}, deg	8.35	8.35	8.35	8.35	8.35	8.35	5	15
Root chord, in.	162.9	152.1	143.4	164.1	167.6	158.3	163.5	161.7
Break chord, in.	42.4	45.7	48.4	43.5	40.9	43.8	43.0	41.1
Tip chord, in.	9.3	12.6	15.3	6.1	7.9	10.7	7.6	12.8

The wing weight for each planform was calculated from the wing-weight equations in FLOPS. Wing weight is dependent on planform shape, load path sweep, and flap area. The inboard sweep of the load path was defined as 0° for all planforms except one, which had a 10° inboard trailing-edge sweep (number 6) for which the load path sweep was 10°. The outboard load path sweep was assumed to be equal to the sweep of the three-quarter chord to allow room for trailing-edge flaps on the outboard portion. Weight increments due to flaps were again assumed to be the same for all the planforms. The wing-weight sensitivity was determined by incrementing the wing weight in FLOPS by 1000 lb and calculating a new

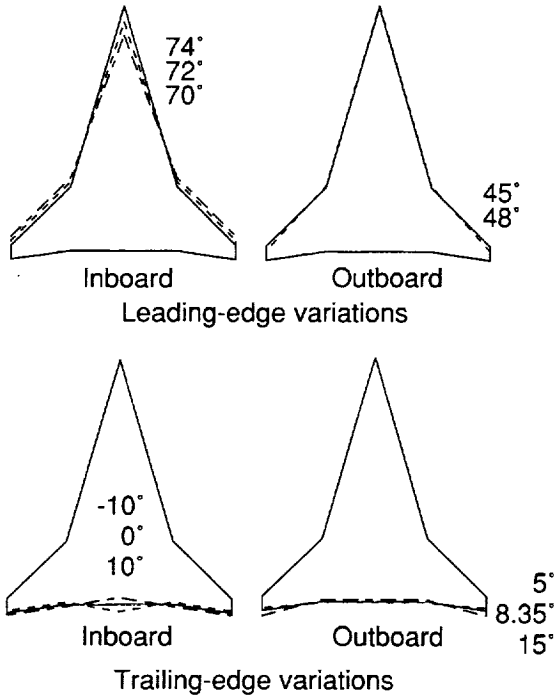

Figure B2. Planform variations.

TOGW. It was determined that TOGW increased by 2.34 lb for every 1-lb increase in wing weight.

The drag due to lift at cruise conditions was calculated with the method of reference 8 for each planform studied. Assuming midcruise design conditions of 62 000 ft and 450 000 lb at Mach 2.4, the camber distribution for each planform was optimized for cruise at a lift coefficient of 0.09. The drag-due-to-lift polar at cruise (Mach 2.4 only) for each planform was entered into FLOPS to determine the sensitivity of the overall aircraft TOGW to supersonic drag due to lift. It was found that one count of drag due to lift at cruise was equivalent to 4500 lb in TOGW.

A generic fuselage, with a length of 300 ft and a volume of 23 000 ft^3, was optimized at Mach 2.4 in the presence of each wing, keeping a minimum cross section constraint of 100 ft^2 on the cabin section of the fuselage while maintaining a constant volume. The aerodynamic center at Mach 0.3 was found for each wing and used to determine the longitudinal placement of the wing on the fuselage. Each wing was placed so that its aerodynamic center was 163 ft back from the nose of the body. The side of body juncture was selected to be at a buttock line of 6 ft. Only the portion of the wing outboard of 6 ft was modeled for wave-drag analysis. Engine nacelles and the vertical tail surface were not included in the wave-drag optimization and estimates. Zero-lift wave-drag values for the wing-fuselage combination were used to determine incremental effects for the configuration. FLOPS was used to determine the sensitivity of the overall aircraft takeoff gross weight to a one-count increment in wave drag applied at all supersonic Mach numbers. It was determined that one count of zero-lift wave drag was worth 5500 lb in takeoff gross weight.

Skin-friction, form, and roughness drag values at cruise conditions were calculated with CDM for each wing-body pair. The effect of these drag increments on takeoff gross weight was determined by adjusting the wetted area ratio parameter in FLOPS to yield a one-count change in skin-friction, form, and roughness drag at the midcruise condition. This had the effect of changing the drag at all Mach numbers. It was determined that one count of skin-friction drag resulted in a 6000-lb change in takeoff gross weight.

Figures B3 through B6 show the individual wing-weight and drag components, overlaid for each sweep, to illustrate the dominant effects on TOGW. All increments in TOGW are referenced to the NASA baseline configuration. The weight increments due to inboard leading-edge sweep are dominated by wave drag, which has twice the effect of the other components. The largest change in TOGW due to outboard leading-edge sweep results from wing weight. For inboard trailing-edge sweep, induced drag shows the largest weight increment, while wave drag is again the largest contributor for outboard trailing-edge sweep.

Figures B7 through B10 show the combined effects of sweep changes on TOGW. As expected from the individual trends presented in figures B3 through B6, inboard leading-edge sweep has the dominant effect on TOGW. Overall, a 1° increase in inboard leading-edge sweep would result in a savings of 8500 lb in TOGW. The effect on TOGW of

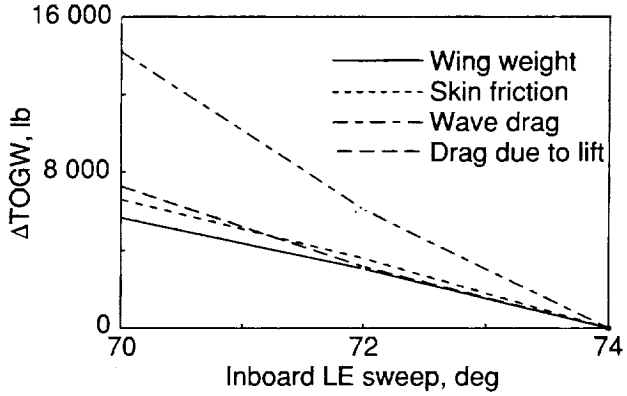

Figure B3. Weight increments due to inboard LE sweep.

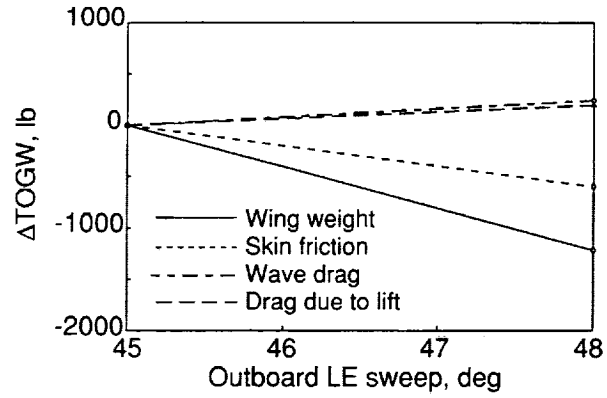

Figure B4. Weight increments due to outboard LE sweep.

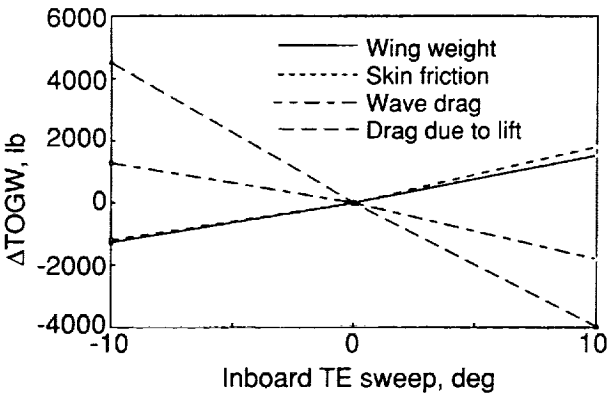

Figure B5. Weight increments due to inboard TE sweep.

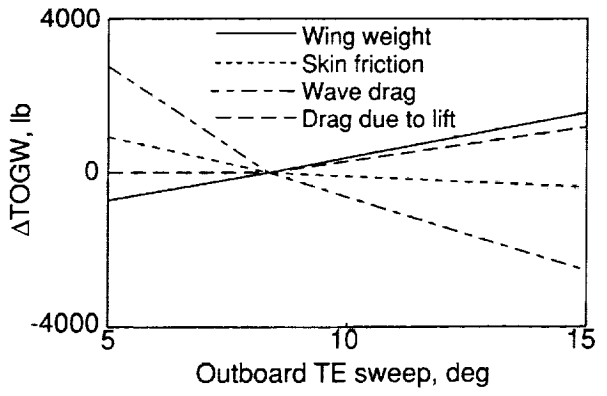

Figure B6. Weight increments due to outboard TE sweep.

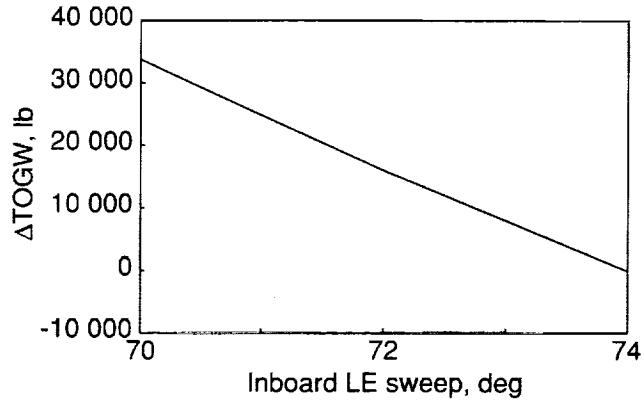

Figure B7. Effect of inboard LE sweep on TOGW.

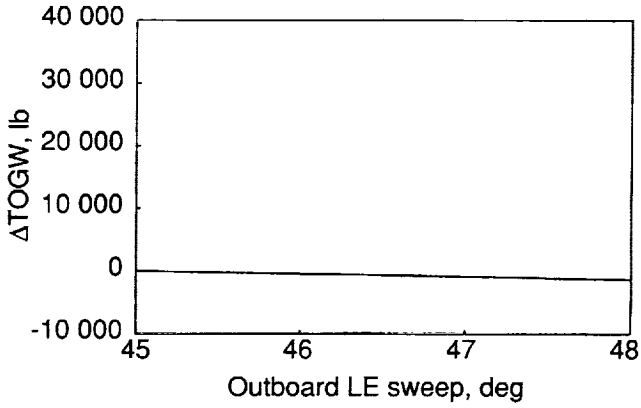

Figure B8. Effect of outboard LE sweep on TOGW.

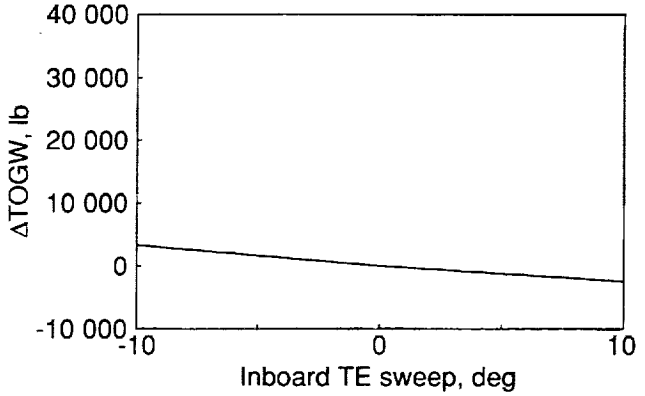

Figure B9. Effect of inboard TE sweep on TOGW.

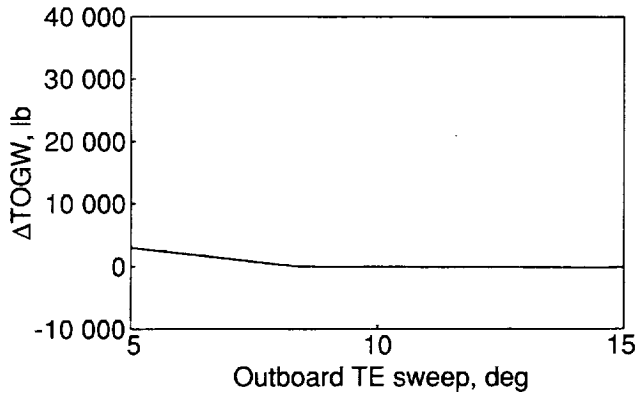

Figure B10. Effect of outboard TE sweep on TOGW.

changes in leading-edge outboard sweep and trailing-edge sweep both inboard and outboard tends to be quite small. The contributions to TOGW from wing weight and skin friction tend to offset those from zero-lift wave drag and supersonic drag due to lift to result in very little change per degree of sweep change.

Overall, the results followed expected trends. Larger values of inboard leading-edge sweep have longer lifting lengths and larger inboard panel areas. As expected, reductions in supersonic drag due to lift, zero-lift wave drag, skin-friction drag, and wing weight were seen in the data. An increase in outboard leading-edge sweep caused a much smaller increase in lifting length and area of the inboard panel than changes due to inboard leading-edge sweep, and similar but less pronounced trends resulted. Increases in inboard and outboard trailing-edge sweep resulted in a longer lifting length and smaller inboard panel for both cases. Such changes were expected to increase wing weight and skin-friction drag while decreasing drag due to lift and zero-lift wave drag, trends that were consistent with the results.

The results of this study provided some basic guidelines for the development of a planform for a high-speed civil transport. When balancing high-speed performance with acceptable low-speed characteristics, these results provided a means of weighing the effects of planform sweeps on the overall configuration.

It has been shown that the greatest effect on TOGW results from the inboard leading-edge sweep for the range of planform sweeps examined. The high leading-edge sweep also affects the characteristics of the low-speed, vortex-dominated flow field, which was not easily estimated by simple methods. An effort to quantify the effects of inboard leading-edge sweep on the low-speed, high-lift characteristics of HSCT configurations is the focus of an ongoing experimental program.

Based on this study, no changes were made to the baseline planform. The inboard leading-edge sweep showed a trend of better performance with higher sweep angle; however, angles greater than 74° were eliminated because the tip chords became unreasonably small when the span was held constant. The other three sweep angles studied showed relatively small effects on vehicle performance and were therefore selected to enhance low-speed considerations and structural feasibility.

References

1. Boeing Commercial Airplane Co.: *High-Speed Civil Transport Study—Summary.* NASA CR-4234, 1989.

2. LTV Aerospace Corp.: *Advanced Supersonic Technology Concept Study Reference Characteristics.* NASA CR-132374, 1973.

3. McCullers, L. A.: Aircraft Configuration Optimization Including Optimized Flight Profiles. *Recent Experiences in Multidisciplinary Analysis and Optimization,* Jaroslaw Sobieski, compiler, NASA CP-2327, Part 1, 1984, pp. 395–412.

4. Cronin, M. J.; Hays, A. P.; Green, F. B.; Radovcich, N. A.; Helsley, C. W.; and Rutchik, W. L.: *Integrated Digital/Electric Aircraft Concepts Study.* NASA CR-3841, 1985.

5. Sommer, Simon C.; and Short, Barbara J.: *Free-Flight Measurements of Turbulent-Boundary-Layer Skin Friction in the Presence of Severe Aerodynamic Heating at Mach Numbers From 2.8 to 7.0.* NACA TN 3391, 1955.

6. *USAF Stability and Control Datcom.* Contracts AF33(616)-6460 and F33615-76-C-3061, McDonnell Douglas Corp., Oct. 1960. (Revised Apr. 1978.)

7. Killian, M. J.: *IDAS Configuration Definition Module User's Manual (CDM).* NA-82-467 (Tasks II.D and III.D of Contract F33615-80-C-3012), Volume II, Rockwell International, Apr. 30, 1992.

8. Carlson, Harry W.; and Darden, Christine M.: *Validation of a Pair of Computer Codes for Estimation and Optimization of Subsonic Aerodynamic Performance of Simple Hinged-Flap Systems for Thin Swept Wings.* NASA TP-2828, 1988.

9. Carlson, Harry W.; and Mann, Michael J.: *Survey and Analysis of Research on Supersonic Drag-Due-to-lift Minimization With Recommendations for Wing Design.* NASA TP-3202, 1992.

10. Middleton, W. D.; and Lundry, J. L.: *System for Aerodynamic Design and Analysis of Supersonic Aircraft. Part 1—General Description and Theoretical Development.* NASA CR-3351, 1980.

11. Middleton, W. D.; Lundry, J. L.; and Coleman, R. G.: *System for Aerodynamic Design and Analysis of Supersonic Aircraft. Part 2—User's Manual.* NASA CR-3352, 1980.

12. Carlson, Harry W.; Darden, Christine M.; and Mann, Michael J.: *Validation of a Computer Code for Analysis of Subsonic Aerodynamic Performance of Wings With Leading- and Trailing-Edge Flaps With a Canard or Horizontal-Tail Surface and an Application to Optimization.* NASA TP-2961, 1990.

13. Onat, E.; and Klees, G. W.: *A Method To Estimate Weight and Dimensions of Large and Small Gas Turbine Engines.* NASA CR-159481, 1979.

14. Ball, W. H.; and Atkins, R. A., Jr.: Rapid Evaluation of Propulsion System Effects. Volume 2: PIPSI Users Manual. AFFDL-TR-78-91-VOL-2, U.S. Air Force, July 1978. (Available from DTIC as AD B031 766L.)

15. Ball, W. H.: Rapid Evaluation of Propulsion System Effects. Volume 4: Library of Configurations and Performance Maps. AFFDL-TR-78-91-VOL-4, U.S. Air Force, July 1978. (Available from DTIC as AD B031 555L.)

16. Fishbach, Laurence H.; and Gordon, Sanford: NNEPEQ: *Chemical Equilibrium Version of the Navy/NASA Engine Program.* NASA TM-100851, 1988.

17. Walkley, K. B.; Espil, G. J.; Lovell, W. A.; Martin, G. L.; and Swanson, E. E.: *Concept Development of a Mach 2.7 Advanced Technology Transport Employing Wing-Fuselage Blending.* NASA CR-165739, 1981.

REPORT DOCUMENTATION PAGE

Form Approved
OMB No. 0704-0188

1. AGENCY USE ONLY *(Leave blank)*	2. REPORT DATE	3. REPORT TYPE AND DATES COVERED
	December 1999	Technical Publication

4. TITLE AND SUBTITLE
Concept Development of a Mach 2.4 High-Speed Civil Transport

5. FUNDING NUMBERS
WU 537-01-22-02

6. AUTHOR(S)
James W. Fenbert, Lori P. Ozoroski, Karl A. Geiselhart, Elwood W. Shields, and Marcus O. McElroy

7. PERFORMING ORGANIZATION NAME(S) AND ADDRESS(ES)
NASA Langley Research Center
Hampton, VA 23681-2199

8. PERFORMING ORGANIZATION REPORT NUMBER
L-17237

9. SPONSORING/MONITORING AGENCY NAME(S) AND ADDRESS(ES)
National Aeronautics and Space Administration
Washington, DC 20546-0001

10. SPONSORING/MONITORING AGENCY REPORT NUMBER
NASA/TP-1999-209694

11. SUPPLEMENTARY NOTES
Fenbert and McElroy: Langley Research Center, Hampton, VA; Ozoroski, Geiselhart, and Shields: Lockheed Engineering & Sciences Company, Hampton, VA.

12a. DISTRIBUTION/AVAILABILITY STATEMENT
Unclassified–Unlimited
Subject Category 05 Distribution: Nonstandard
Availability: NASA CASI (301) 621-0390

12b. DISTRIBUTION CODE

13. ABSTRACT ***(Maximum 200 words)***
In support of the NASA High-Speed Research Program, a Mach 2.4 high-speed civil transport concept was developed to serve as a baseline for studies to assess advanced technologies required for a feasible year 2005 entry-into-service vehicle. The configuration was designed to carry 251 passengers at Mach 2.4 cruise with a 6500-n.mi. range and operate in the existing world airport structure. The details of the configuration development, aerodynamic design, propulsion system and integration, mass properties, sizing, and mission performance are presented. The baseline configuration has a wing area of 9100 ft^2 and a takeoff gross weight of 614 300 lb. The four advanced turbine bypass engines have 39 000 lb thrust with a weight of 9950 lb each, yielding a vehicle takeoff thrust-to-weight ratio of 0.254 and a takeoff wing loading of 67.5 lb/ft^2. The configuration was sized by the 11 000-ft takeoff field length requirement and the usable fuel volume limit, which results in a rotation speed of 179 knots and an end-of-mission landing approach velocity of 134 knots.

14. SUBJECT TERMS	15. NUMBER OF PAGES
Supersonic cruise; Aircraft design; Transport aircraft	31
	16. PRICE CODE: A03

17. SECURITY CLASSIFICATION OF REPORT	18. SECURITY CLASSIFICATION OF THIS PAGE	19. SECURITY CLASSIFICATION OF ABSTRACT	20. LIMITATION OF ABSTRACT
Unclassified	Unclassified	Unclassified	UL